Room-temperature ductility enhancement of Mo alloy with nano-sized metal oxide dispersions

N. Ma, and B.R. Cooper
Physics Department
West Virginia University

C. Feng, J. Tannenbaum and B.S.-J. Kang
Mechanical and Aerospace Engineering Department
West Virginia University

22nd Annual Conference on Fossil Energy Materials, Pittsburgh, July 8-10, 2008

DOE/NETL ARM Program, contract no. DE-AC05-00OR22725 managed by UT-Battelle, LLC
(6/23/2005 to 6/30/2008)

And

DOE/NETL UCR Program, contract no. DE-FG26-05NT42526 (8/01/2005 to 7/31/2008)
Patricia Rawls, Program Manager

Research Objective: To understand and to remedy the impurity effects for room-temperature ductility enhancement of molybdenum (Mo) based alloys by the inclusion of candidate nano-sized metal oxide dispersions.

Task 1: Molecular Dynamic Simulation

To study ***microscopic*** mechanisms of impurity embrittlement of **Mo**- and **Cr**-based alloys and their room-temperature ductility enhancement effects of **MgO** or **$MgAl_2O_4$**.

To develop predictive capabilities to facilitate the design and optimization of Mo and other high temperature alloys for fossil energy materials applications.

Task 2: In-situ Mechanical Property Measurement

To develop a micro-indentation measurement technique ** for quick assessment of material mechanical behavior and properties. Task 2 also includes preliminary development of Mo alloys with candidate nano-sized metal oxides (**$MgAl_2O_4$**)

** : Also co-supported by NETL, Materials and Component Development for Advanced Turbine Systems Program, Project Monitor: Mary Anne Alvin

Background

Due to their ultra-high working temperature (>1000oC) and excellent oxidation and corrosion resistance, a number of Cr and Mo based alloys are being developed as the next generation structural materials for fossil energy applications. However, a severe drawback with these materials is their limited room temperature ductility.

Past studeis showed ductility improvement of Mo phase by inclusion of metal oxide dispersion (e.g. Schnibel 2003)

Experimental difficulties:

- Optimal dispersion **composition**
  - $MgAl_2O_4$, MgO, or other oxide candidates?
  - nano-size oxide? how to achieve uniform dispersion and prevent agglomeration?

Atomistic modeling can provide some answers to these questions to reduce experimental trial and error

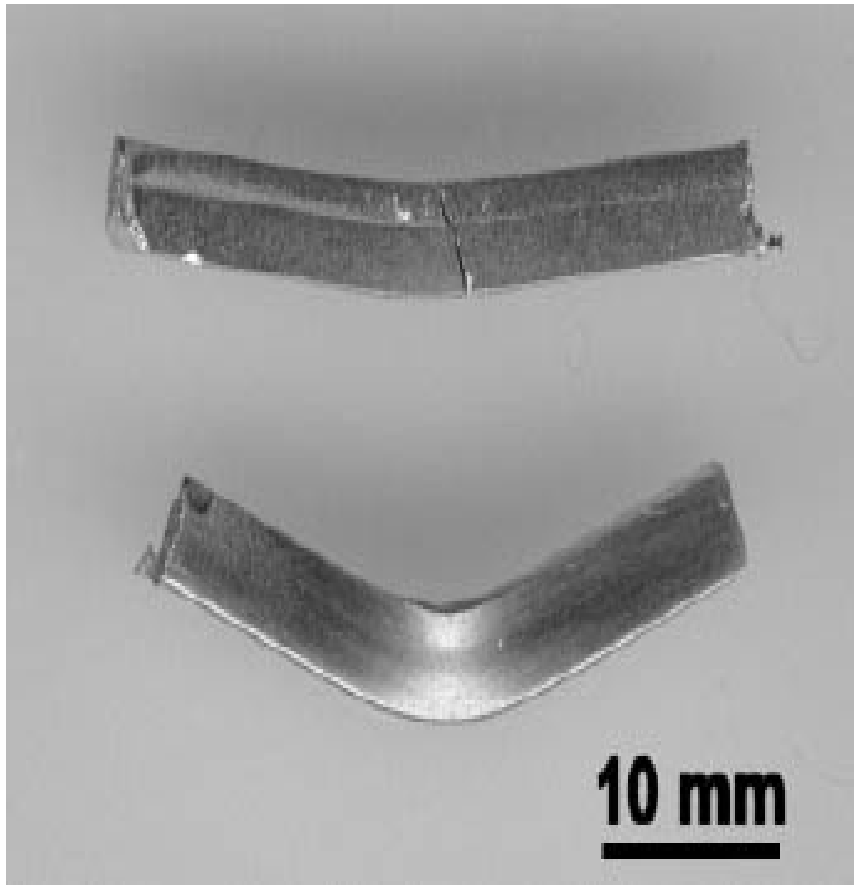

Mo with spinel dispersions: different procedures yield different results. (Schnibel, 2003)

Influence of impurity elements

Insufficient ductility mostly due to impurities (such as N, O, etc.)

- weaken the metal-metal bond
- precipitate or segregate as brittle oxides or nitrides

Ductility enhancement by MgO or $MgAl_2O_4$ spinel dispersions:

- Scruggs 1965: on Cr and Mo Alloys
  - Mechanism assumed to be impurity gettering by spinel phase

- Brady 2003 (detailed microstructural analysis): on Cr Alloys
  - Impurities detected near the metal oxide boundary (not inside the oxide)
    - $MgAl_2O_4$ is not as effective as MgO
    - Other metal oxides were tried with detrimental results
    - unclear whether MgO or $MgCr_2O_4$ is more effective

  - **Fundamental mechanism is not fully understood**
    - Further studies are needed to optimize the composition and size of dispersion material

(Extension of) Rice's criterion

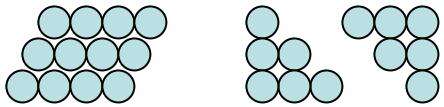

What matters are:

the characteristics of the chemical bonds

the properties of the valence electrons

How properties of electrons affect ductility

In brittle materials …

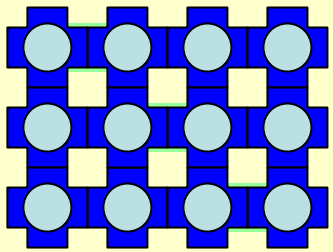

ions
electrons
voids

Localized, immobile electrons form rigid bonds → brittle

Localized around ions

Immobile (cannot fill the voids easily)

Delocalized, mobile electrons make flexible bonds → ductile

(Extension of) Rice's criterion

Delocalized electrons → **ductile**

Mobile electrons → **ductile**

Flexible bonds → **ductile**

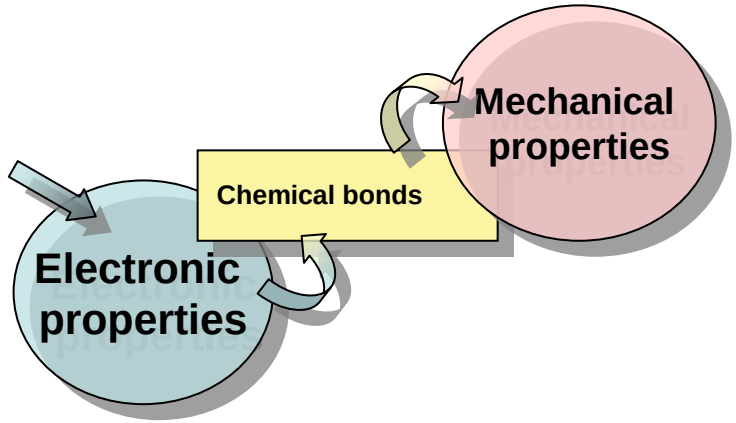

Properties of electrons

- **Space distribution**
  How localized/delocalized electrons are
- **Energy distribution**
  How easy electrons can be excited to mobile states
- **Angular momentum distribution**
  How rigid/flexible chemical bonds are

Model systems

Cr/Mo
N/O
Mg
O

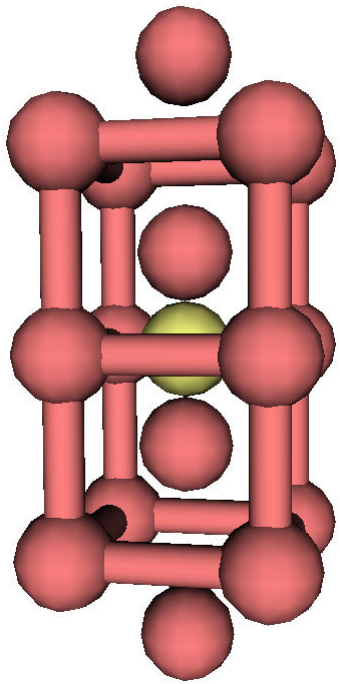

A. impurity embrittled system

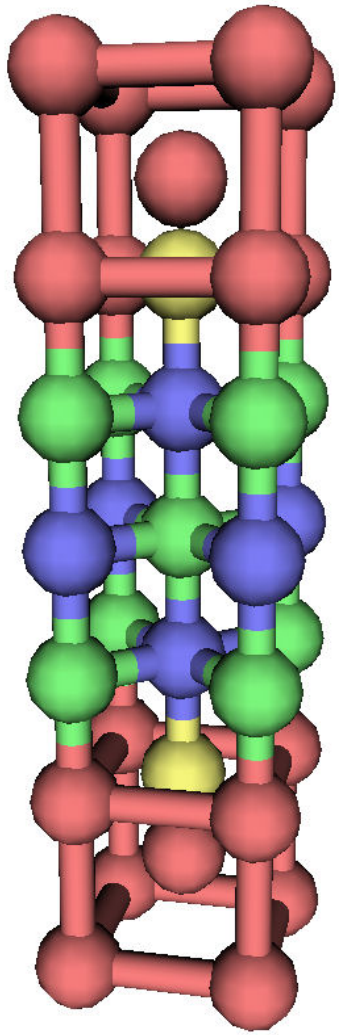

B. ductility enhanced system

Spatial charge distribution

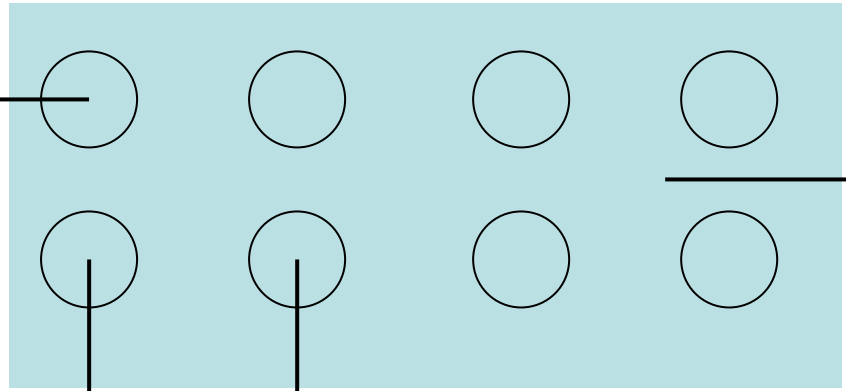

Muffin tin (MT) charge	Interstitial charge
• Localized within ions (yet still can be shared) • Less mobile • Partial contributor	• Fully delocalized • Mobile ('itinerate') • Main contributor to metallic bonds and ductility

more interstitial charge → better ductility

uniformly shared MT charge → better ductility

Results: Interstitial charge (Cr alloys)

more interstitial charge → better ductility

Impurity imbrittled Cr	MgO ductilized Cr

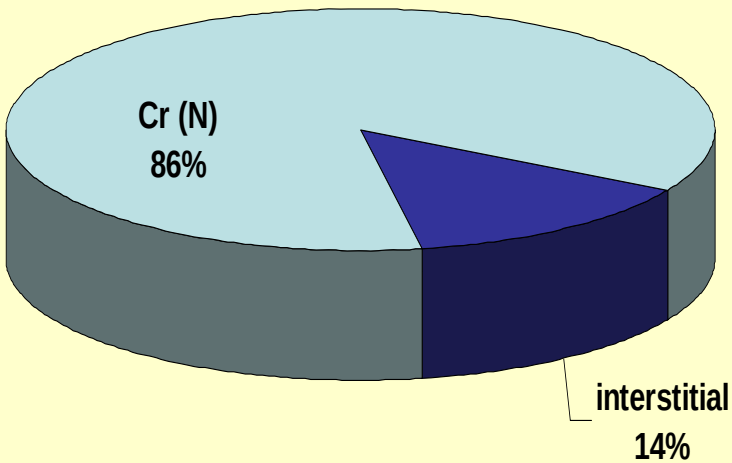

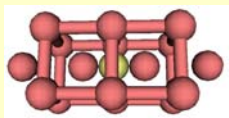

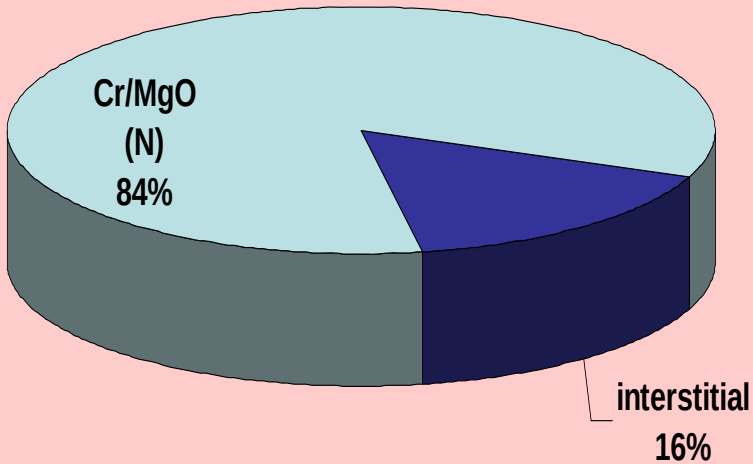

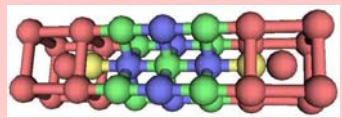

Results: Interstitial charge (Mo alloys)

more interstitial charge → better ductility

Impurity imbrittled Mo	MgO ductilized Mo

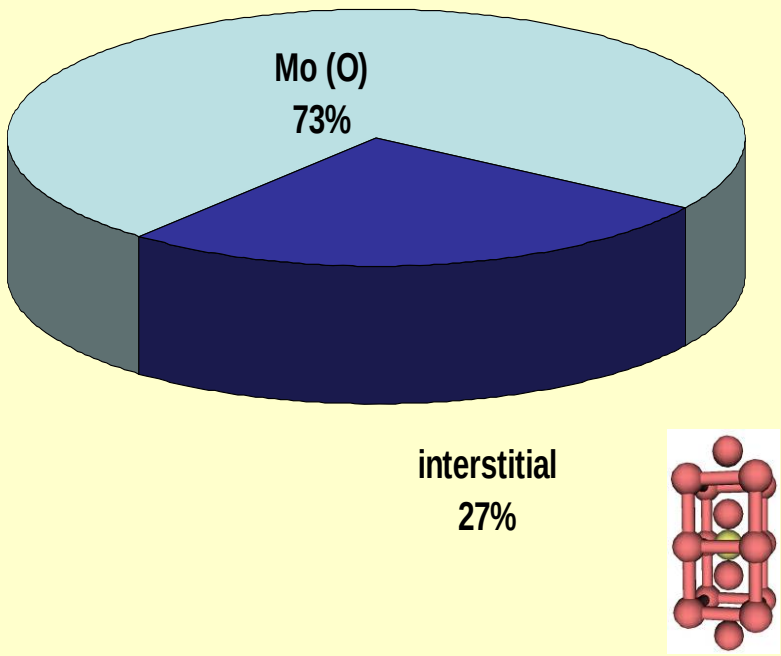

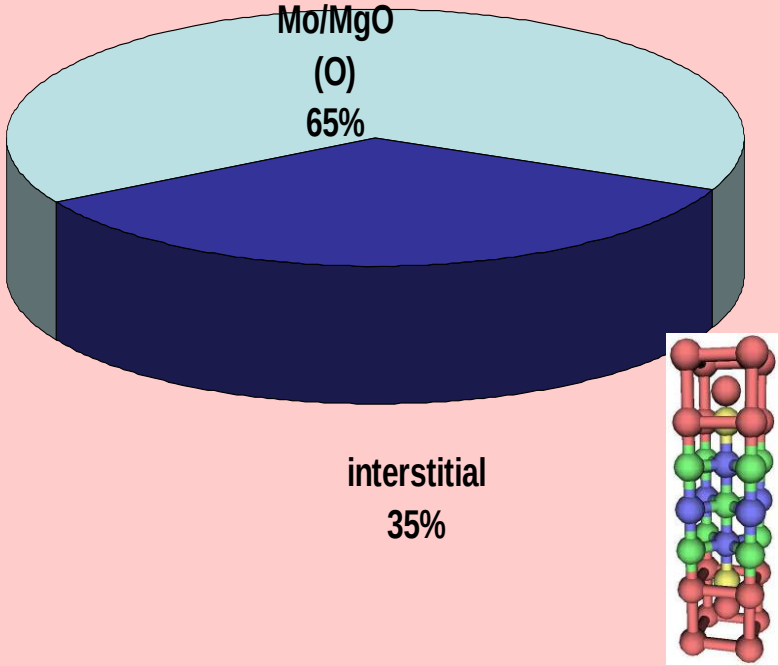

Results: Muffin-tin charge distribution

uniformly shared MT charge (less variance) → better ductility

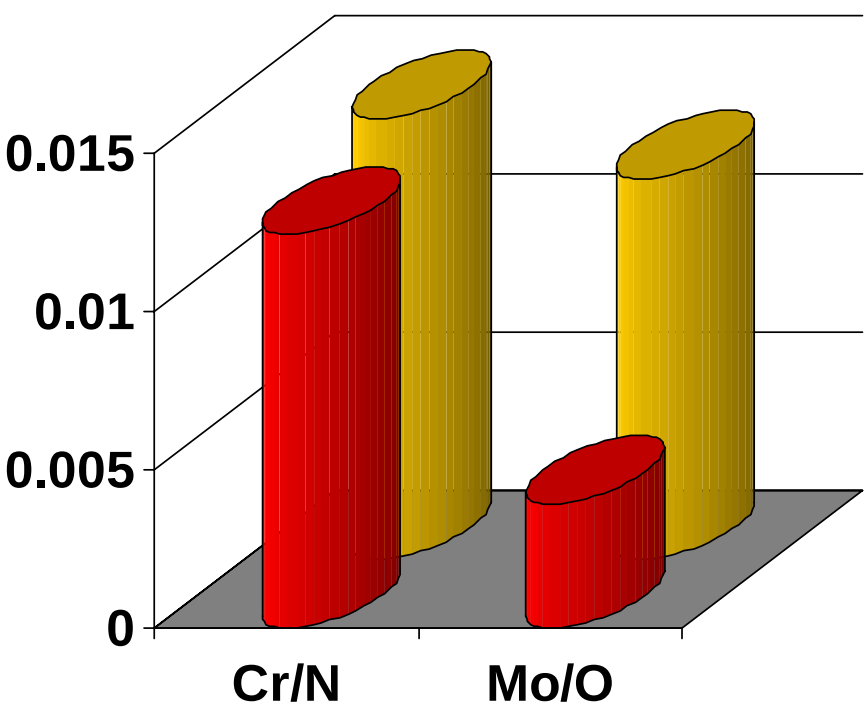

MgO ductilized

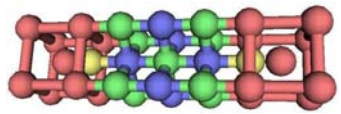

Impurity embrittled

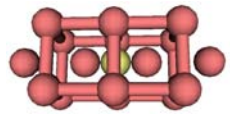

Variance of MT charge distribution among different Cr or Mo ions.

Results: L-projected population

Charge (e)	N imbrittled Cr				MgO ductilized Cr		
	1st Cr	2nd Cr	3rd Cr	4th Cr	1st Cr	2nd Cr	3rd Cr
s-like	0.172	0.260	0.204	0.206	0.256	0.297	0.245
d-like	3.772	3.970	3.603	3.585	4.137	3.998	3.734
s/d %	4.6	6.5	5.7	5.7	6.2	7.5	6.6

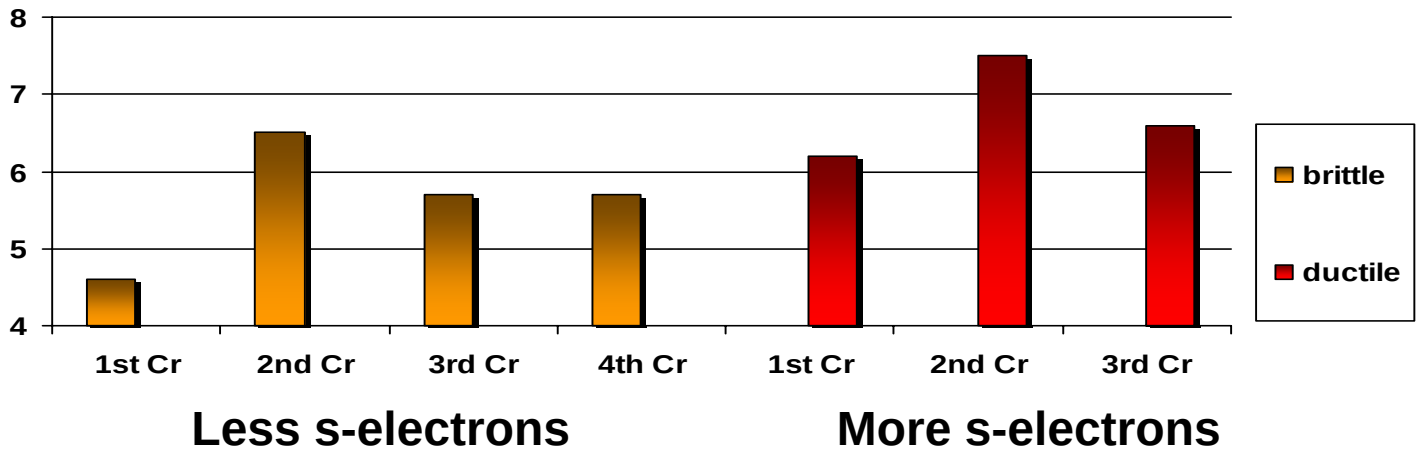

Results: L-projected energy

Energy Ryd.)	O embrittled Mo				MgO ductilized Mo		
	1st Cr	2nd Cr	3rd Cr	4th Cr	1st Cr	2nd Cr	3rd Cr
E* 4s	1.004	0.954	1.078	1.077	0.837	0.940	1.058
E* 3d	0.808	0.730	0.854	0.849	0.868	0.934	1.047
ΔE	0.20	0.22	0.22	0.23	-0.03	0.01	0.01

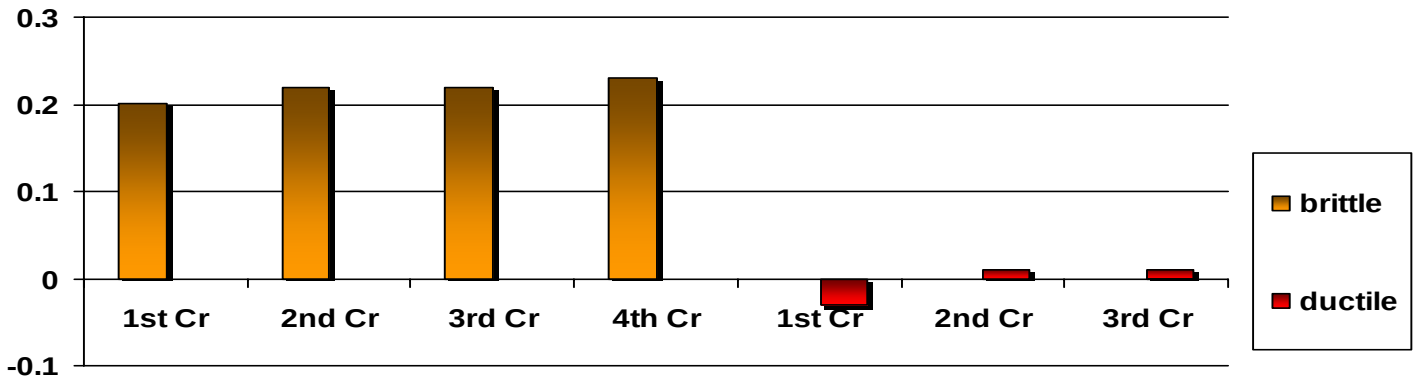

Higher s level **Lower s level**

Summary: Properties of electrons

What has been achieved?

Identified ***microscopic*** criteria
to predict **brittle/ductile** properties

These criteria can

*Explain the **mechanism***
*Be used in larger scale simulations to **optimize** performance*

Result: Molecular Dynamics (Cr/MgO with N)

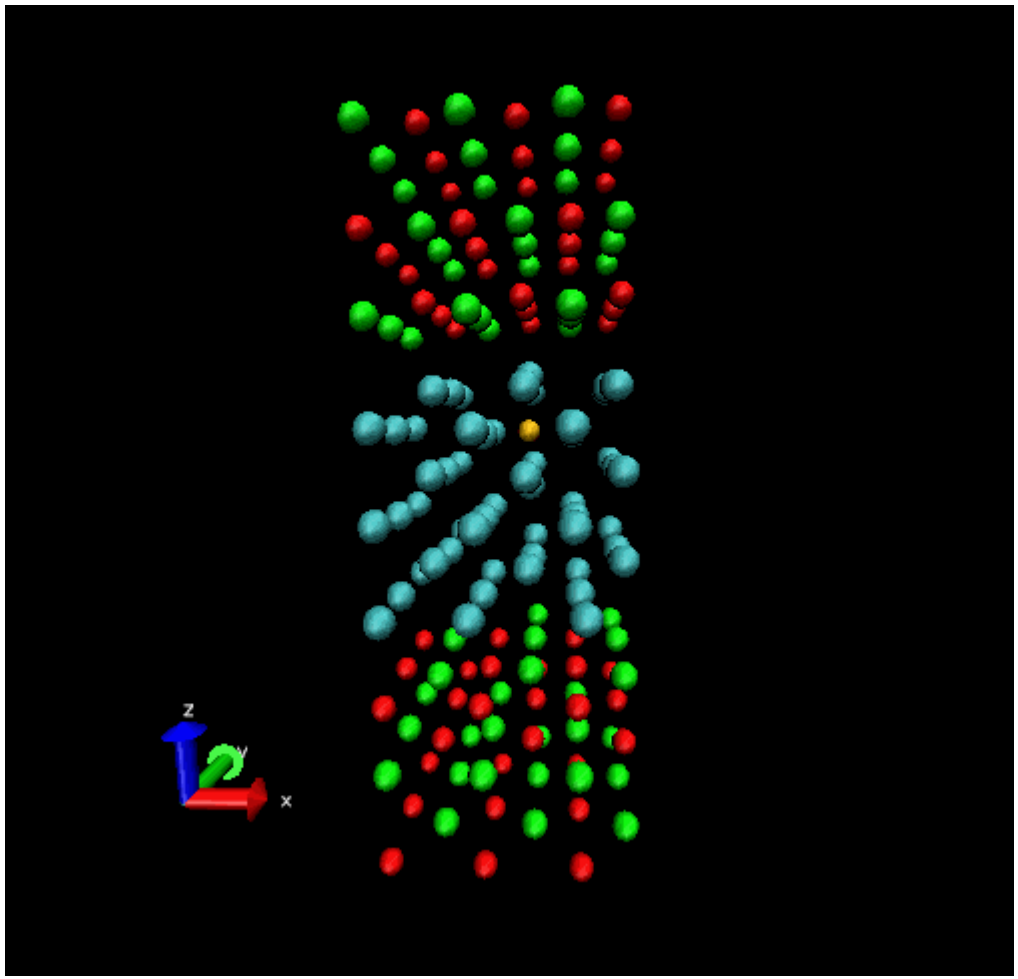

- Cr
- N
- Mg
- O

163 atoms

Constant Temperature (600 K)

Diffusion time ~1ps (10^{-12}s)
Diffusion length ~ 2A

Result consistent with Brady's experiment

Analysis: Charge Density Distribution and DOS

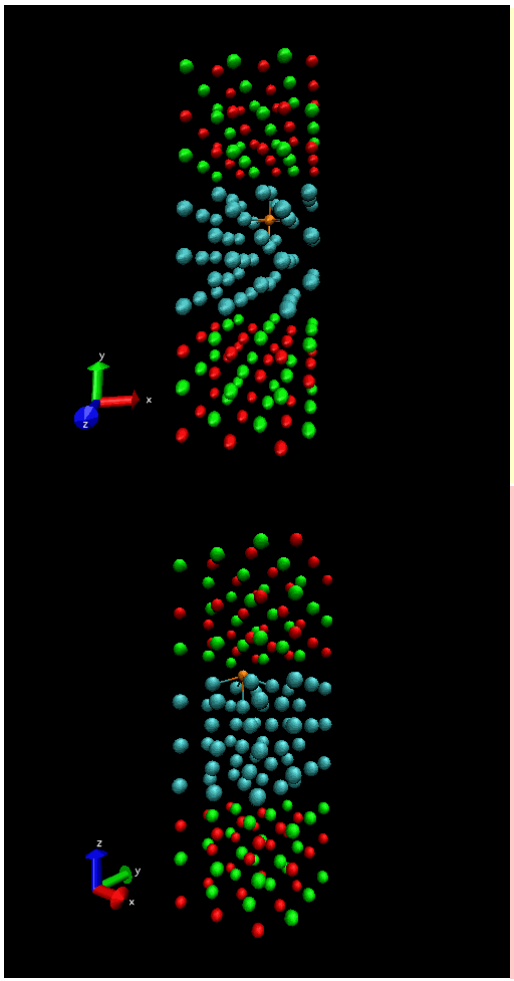

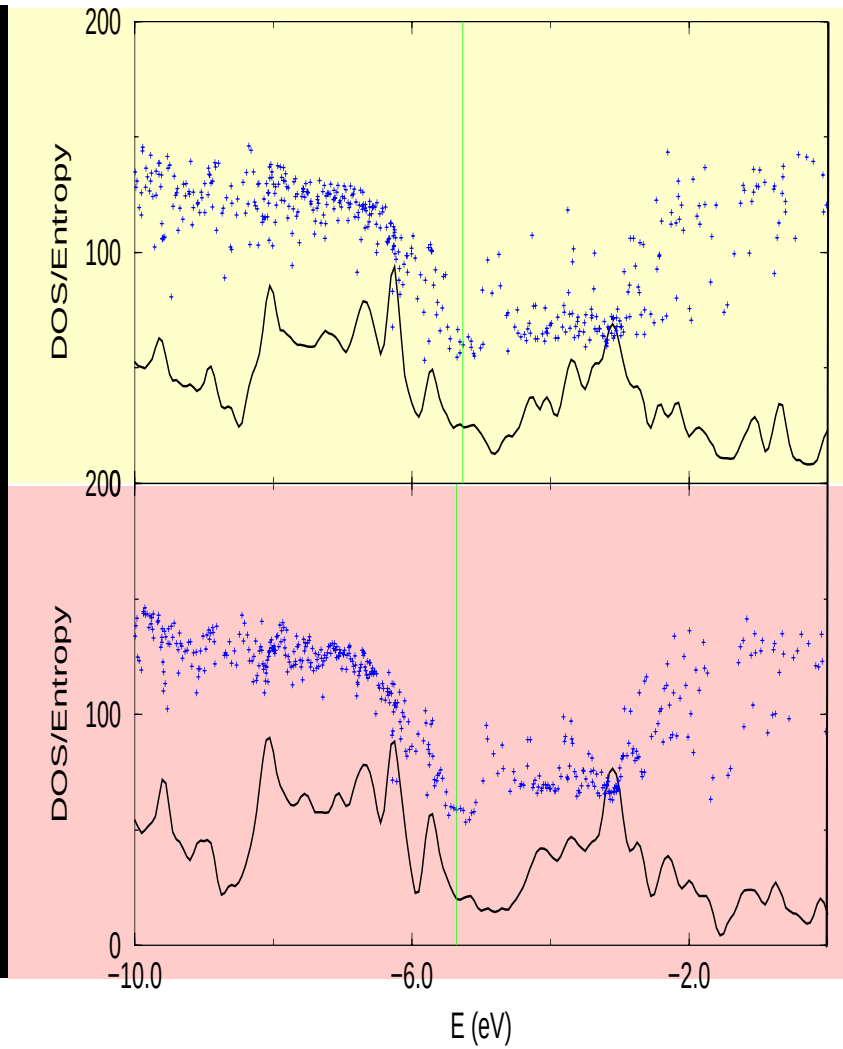

# of states within +/- 1eV of Fermi level

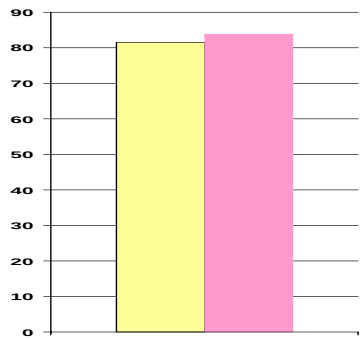

Avg. entropy

Analysis: Impurity Electronic States

In the bulk of Cr

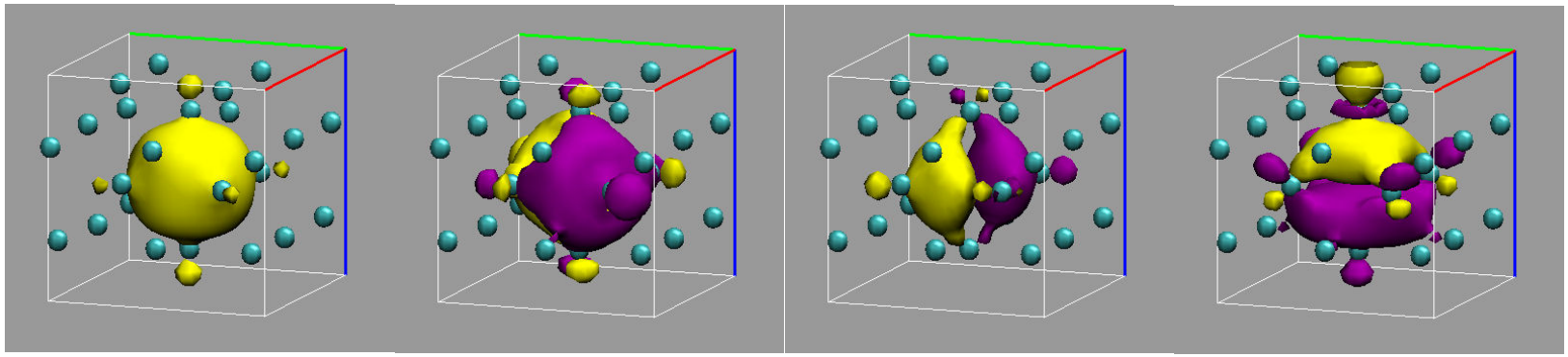

Near the Cr/MgO boundary

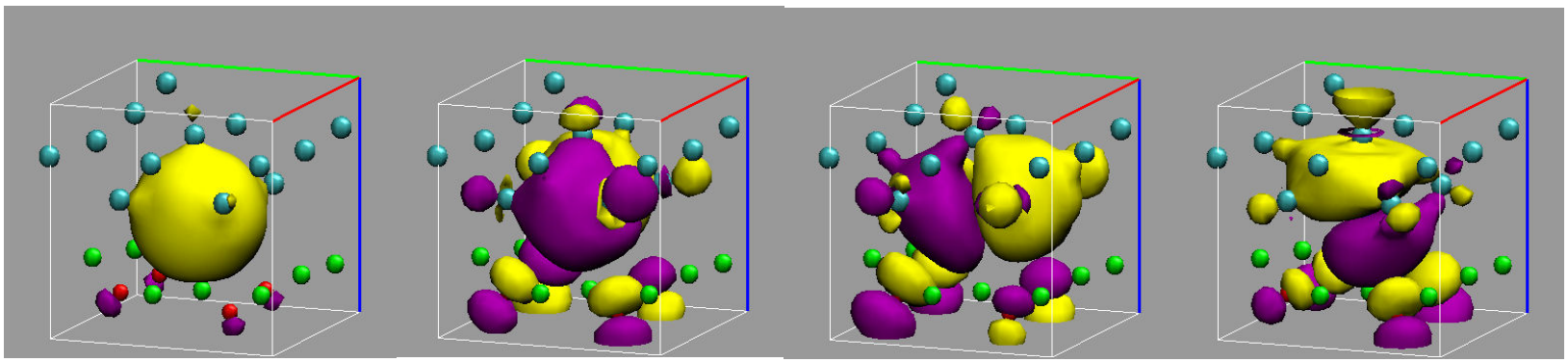

Conclusion: O-N antibonds force the impurity states to rotate 45 degrees, promoting more flexible σ bonds in the system.

Mo/Spinel: Stability of Impurity

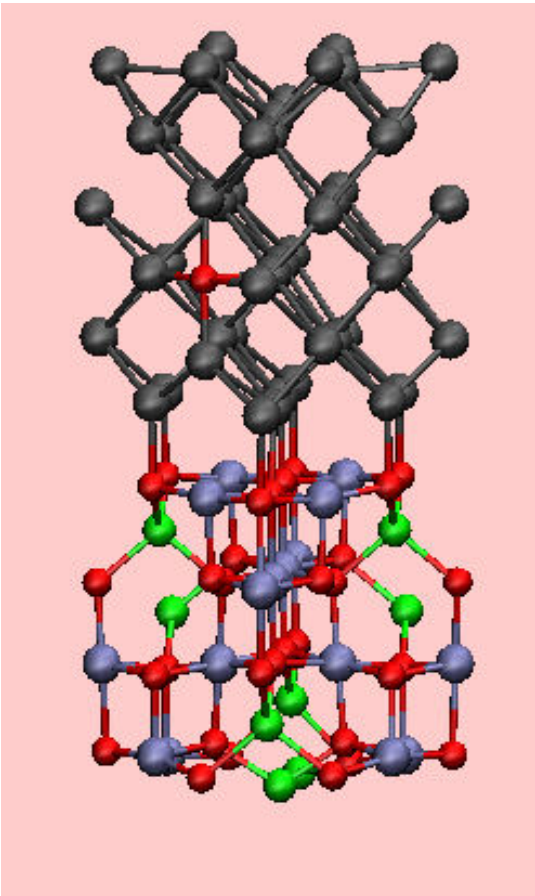

E = -990.2 eV

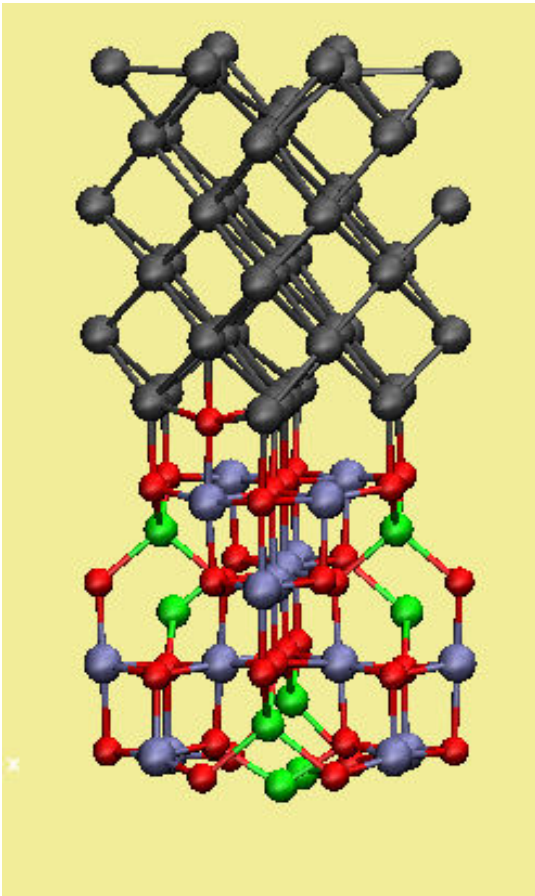

E = -993.0 eV

48 Mo atoms
56 Spinel atoms
1 O impurity

-2.8eV ➔ more stable

Mo/Spinel: L-projected Occupations

	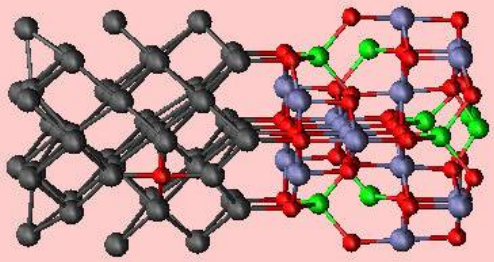	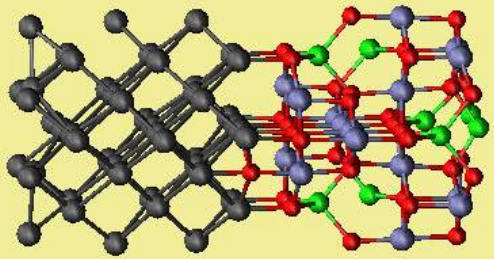	
O 2s	1.60	1.62	+0.02
O 2p	4.61	4.60	- 0.01
Mo 4s	36.53	36.66	+0.13
Mo 3d	250.24	250.04	- 0.20

Mo/Spinel: Average Entropy of the States

	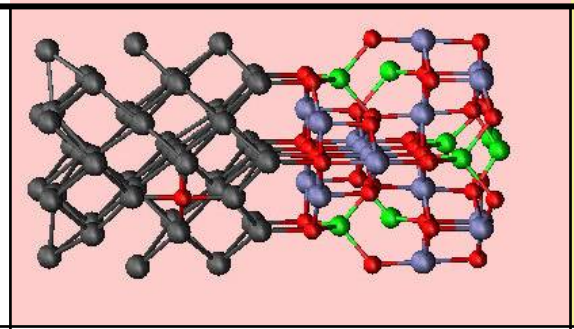	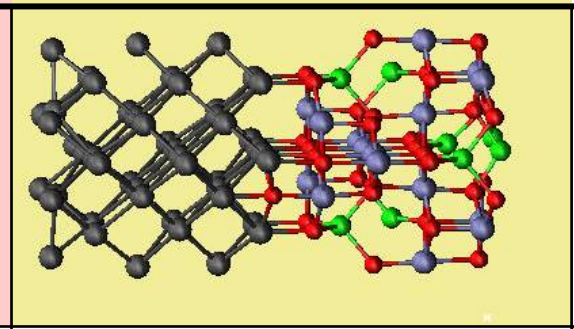	
O	16.4	31.1	+14.7
Mo/48	60.2	61.1	+0.9

Note: higher entropy means more delocalized spatial charge distribution → **more ductile**

Mo/MgO: Stability of Impurity

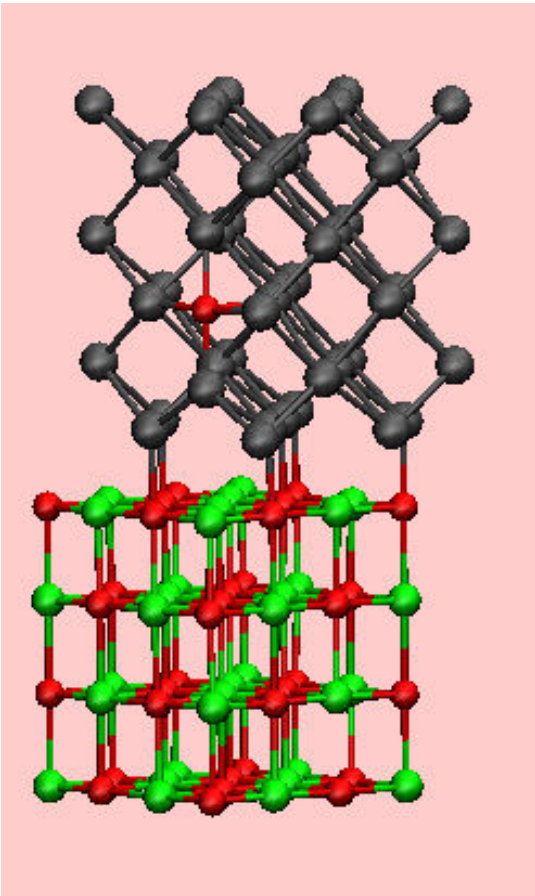

E = -690.2 eV

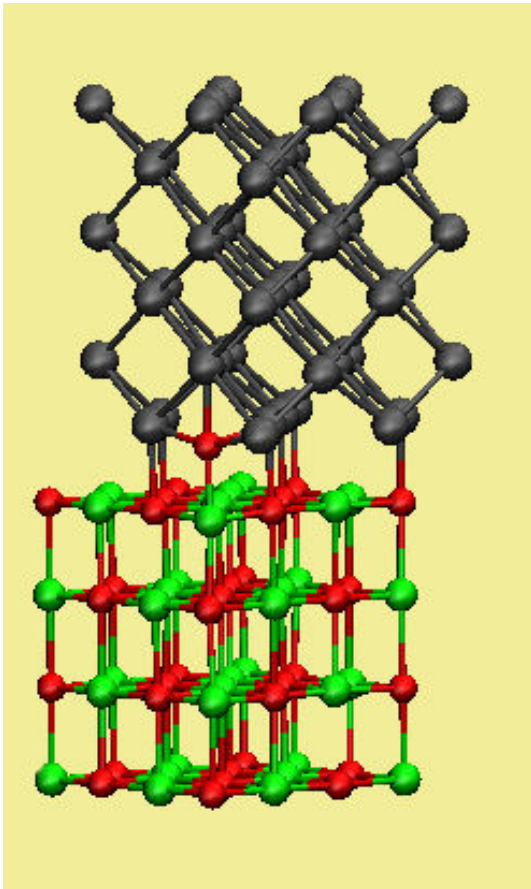

E = -692.3 eV

48 Mo atoms
64 MgO atoms
1 O impurity

-2.1eV ➔ more stable

Mo/MgO: L-projected Occupations

	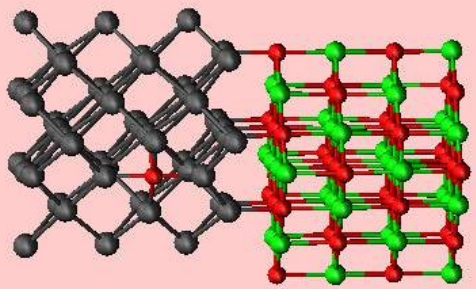	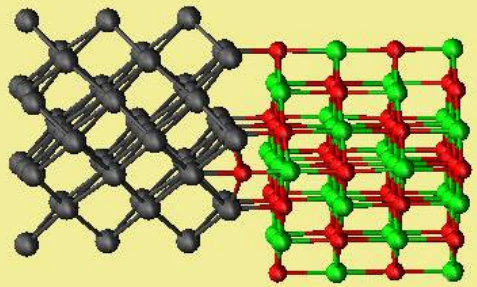	
O 2s	1.56	1.57	+0.01
O 2p	4.64	4.65	+0.01
Mo 4s	35.06	35.09	+0.03
Mo 3d	250.97	250.88	-0.09

Mo/MgO: Average Entropy of the States

	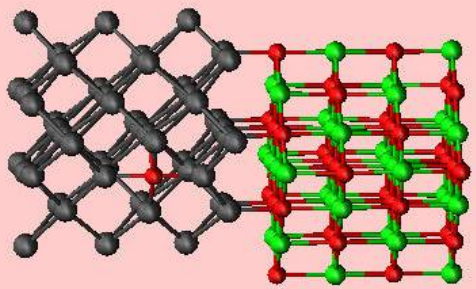	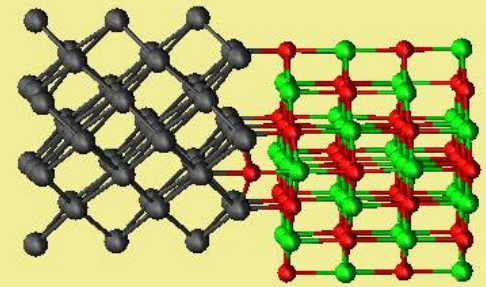	
O	13.2	20.8	+7.6
Mo/48	58.3	57.5	-0.8

Note: higher entropy means more delocalized spatial charge distribution → **more ductile**

Comparison: Spinel vs. MgO

	Spinel		MgO	
O 2s	1.62	+0.02	1.57	+0.01
O 2p	4.60	-0.01	4.65	+0.01
Mo 4s	36.66	+0.13	35.09	+0.03
Mo 3d	250.04	-0.20	250.88	-0.09
O states	31.1	+14.7	20.8	+7.6
Mo states	61.1	+0.9	57.5	-0.8

Conclusion: though both spinel and MgO may enhance the metallic bonds and ductility of Mo, spinel is more efficient than MgO.

Summary: Task 1: Molecular Dynamics Simulation

Cr-based systems: *Observed possible impurity gettering*

- N diffused from inside the matrix to the interfacial boundary
- Charge distribution and DOS properties indicate improved ductility
- Results in consistency with Brady's experimental work:

  "impurity management effects"

  *Brady, et.al. Mat. Sci. & Eng. A, **358**, 243 (2003)*

Mo-based systems: *No impurity gettering observed up to 1000 ^{o}K*

- Higher barrier for oxygen diffusion activation
- Possible ductility enhancement features observed for both spinel and MgO → *delocalized states, higher s occupation ratio, etc.*
- Spinel is more efficient than MgO

Task 2: In-situ mechanical property measurement

Micro-Indentation Technique Development at WVU

- Gen I: Transparent Indenter Measurement (**TIM**) Technique **(Interferometric Indentation Method)**
- Gen II: Contact Area with Multi-partial Unloading Procedure **(A Simplified TIM Method)**
- **Gen III**: Multi-partial Unloading Technique **(A Load-Based Algorithm)**

Capability:

- Young's modulus, hardness, stress-strain curve of alloys or thin-film coating, surface stiffness response measurement of multi- layers structures, e.g. TBC
- **Ductile/Brittle** assessment using indentation technique
  - Indentation-induced surface cracking
  - Surface profile/slip lines/shear bands

Motivation for Micro-Indentation R&D

Material Matrix (typical alloys development)

*Pure Cr, HP 2 hrs/1590C	Cr-6TiO2, HP 2hrs/1590C
*Scruggs Cr-6MgO-0.5Ti (extrusion, 1300C) HP 2hrs/1590C	Cr-6Y2O3, HP 2hrs/1590C
Cr-6MgO-0.5Ti, HP 2hrs/1590C	Cr-2MgO, HP 2hrs/1590C
Cr-6MgO-0.5Ti, sintered HP 2hrs/1590C	Cr-2ZrO2, HP 2hrs/1590C
Cr-6MgO-0.5Ti, HIP 1.5hrs/1590C	Cr-2TiO2, HP 2hrs/1590C
Cr-6MgO-1Ti, HP 2hrs/1590C	Cr-6La2O3, HP 2hrs/1590C
Cr-6MgO-2.2Ti, HP 2hrs/1590C	Cr-3MgAl2O4, HP 2hrs/1590C
Cr-6MgO-0.75Ti, HP 2hrs/1590C, extruded 1300C	Cr-Fe-MgO, 51.75Cr-42.44FE-5.66MgO-0.15La2O3wt%, extruded powders at 1300C
Cr-6MgO-0.75Ti, HP 3hrs/1590C, extruded 1300C	*Cast Re-(26-30)Cr wt% nominal
Cr-6MgO, HP 2hrs/1300C	#695, MO, Mo powder (2~5um) HP/1hr/1800ºC/3ksi/Vacuum
Cr-6MgO, HP 2hrs/1450C	*#697, Mo-6wt%MgAl2O4, Mo powder (2-8um), MgAl2O4 (1-5um) HP/1hr/1800ºC/3ksi/Vacuum
Cr-6MgO, HP 2hrs/1590C	#698, Mo-3wt%MgO, Mo powder (AEE, 2-8um) MgO, HP/1hr/1800ºC/3ksi/Vacuum
*Cr-6MgO(Nano), HP 2hrs/1500C	*#678, Mo-3.4wt%MgAl2O4, Mo powder(2-8um) MgAl2O4(1~5μm),HP/1hr/1800ºC/3ksi/Vacuum

Alloys received from M.P. Brady and J. H. Schneibel, ORNL; HP: Hot Pressed; *: Alloys Tested

Tensile Test Specimen EDM Cutting

3-point bending
test specimen

(Diameter:62mm)
(2.5in)

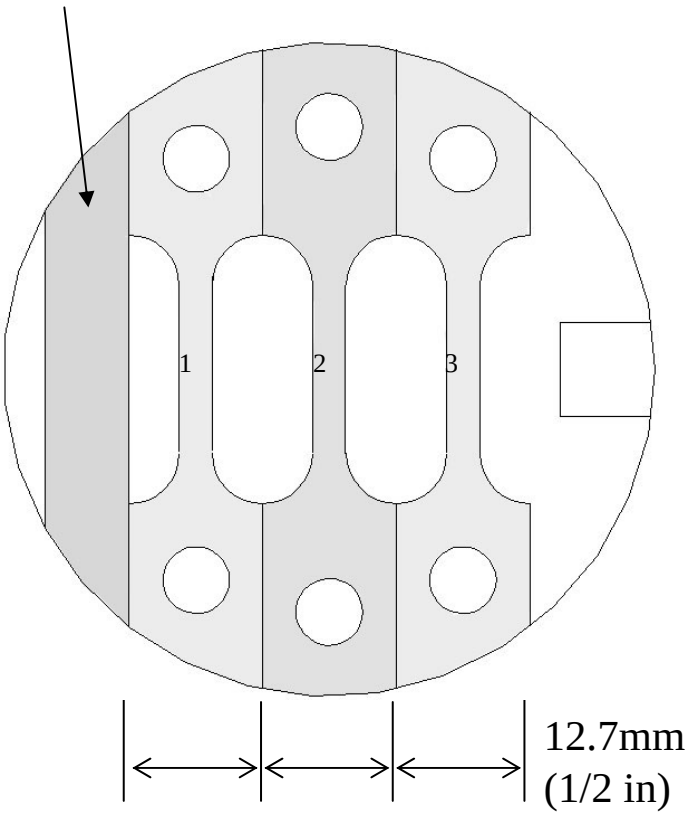

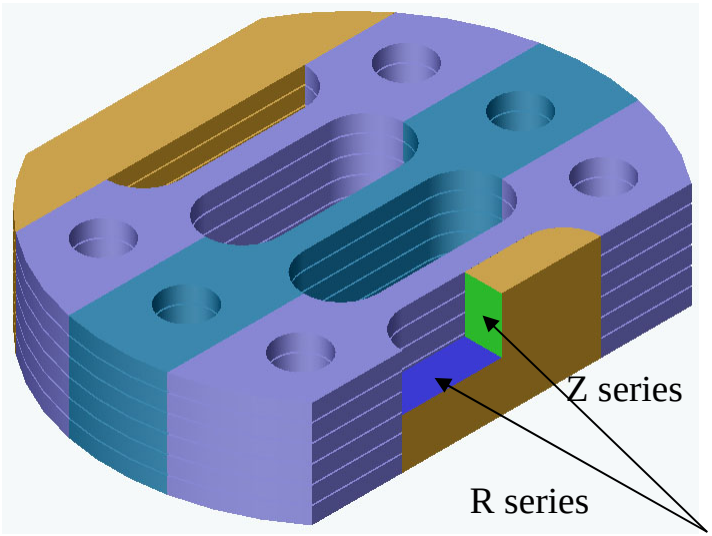

Can be used for microstructure study

High Temperature Tension Test Experimental Setup

MTS 810 System

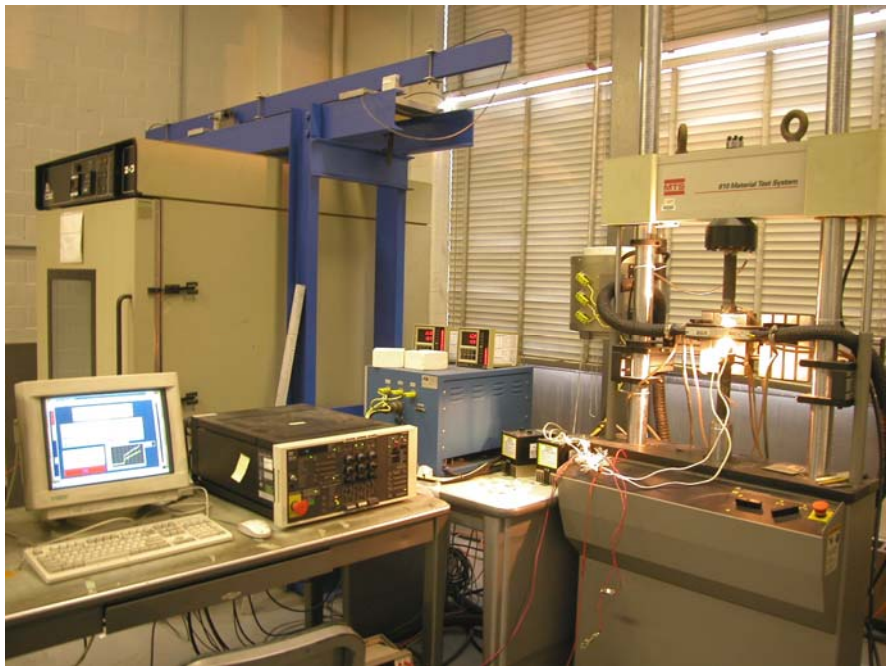

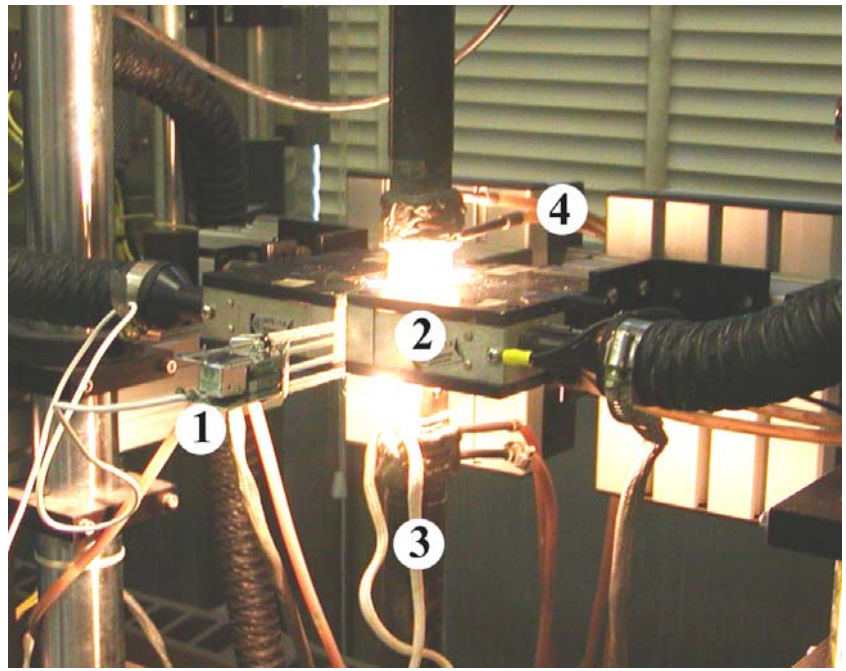

- **MTS 810 high temperature material testing system**

  1. High temperature extensometer, 2. Quartz lamp heater
  3. Thermal couple, 4. Water cooling lines

Alloy #697 Tensile Test Results with Thermal Cycle Effect

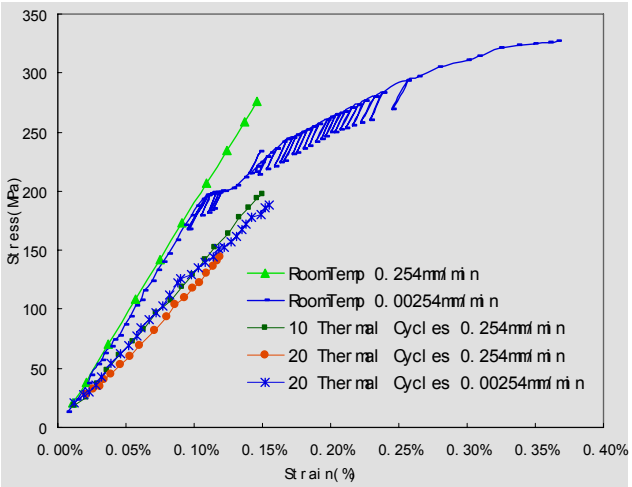

Room Temperature

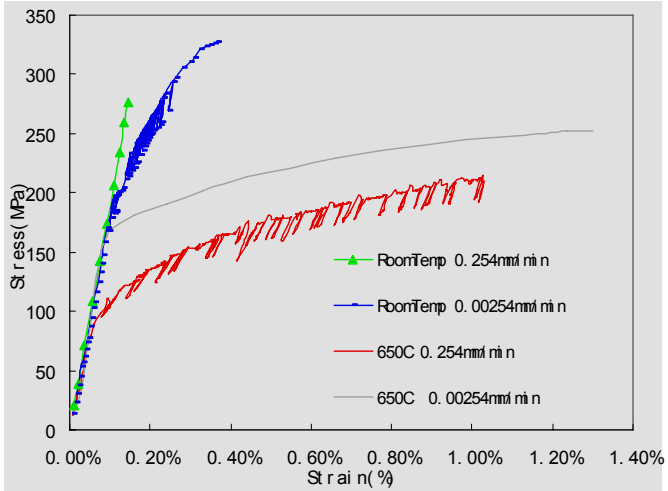

Room Temperature and 650ºC

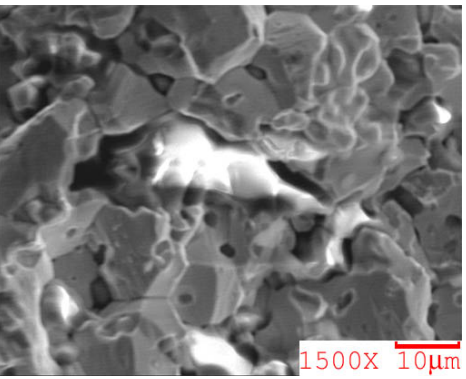

Room Temp
0.254mm/min

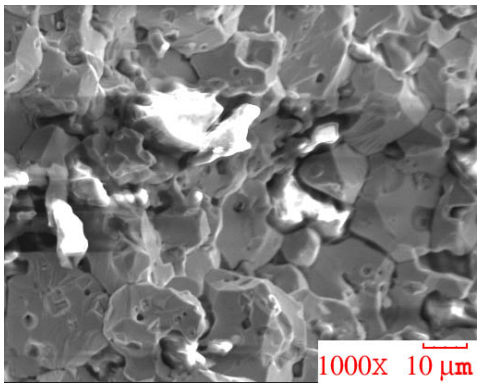

Room Temp
0.00254mm/min

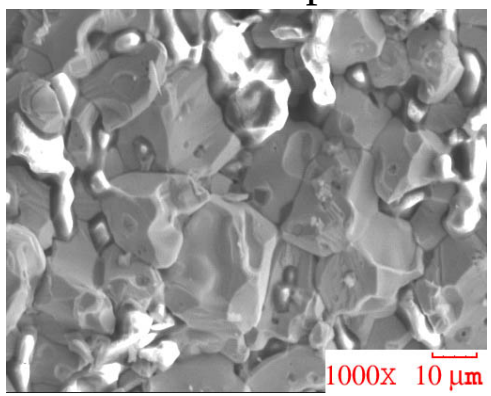

650ºC
0.254mm/min

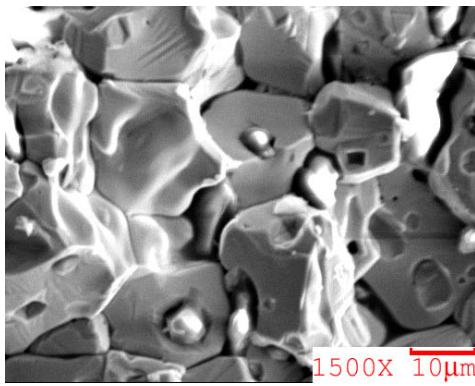

650ºC
0.00254mm/min

Instrumented Indentation Technique
(Background)

- Young's modulus (E)

$$\frac{dP}{dh} = \frac{2}{\sqrt{\pi}} E_r \sqrt{A}$$ (Spherical indentation)

Where *Er* is the reduced Young's modulus,

$$\frac{1}{E_r} = \frac{1-\nu^2}{E} + \frac{1-\nu_0^2}{E_0}$$ (M.F. Doerner et al, 1986)

A: contact region (derived from dp/dh or direct measurement)

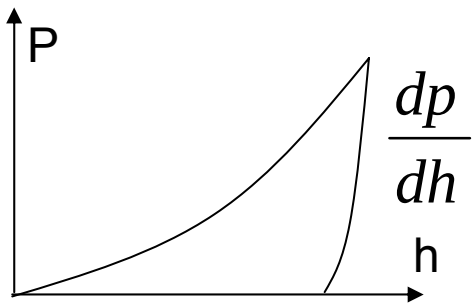

P-h curve from load-depth sensing indentation test

- Post-yielding stress-strain data
  - Tabor's empirical relation:
    d : contact diameter, D *:* indenter diameter, *Pm:* mean pressure *C:* constraint factor.
  - Constraint factor C is strain hardening depended

$$\varepsilon = 0.2\frac{d}{D}$$

$$\sigma = \frac{P_m}{C} \qquad P_m = \frac{Load}{\pi a^2}$$

ORNL Cast Re-(26-30) Cr wt% Alloy

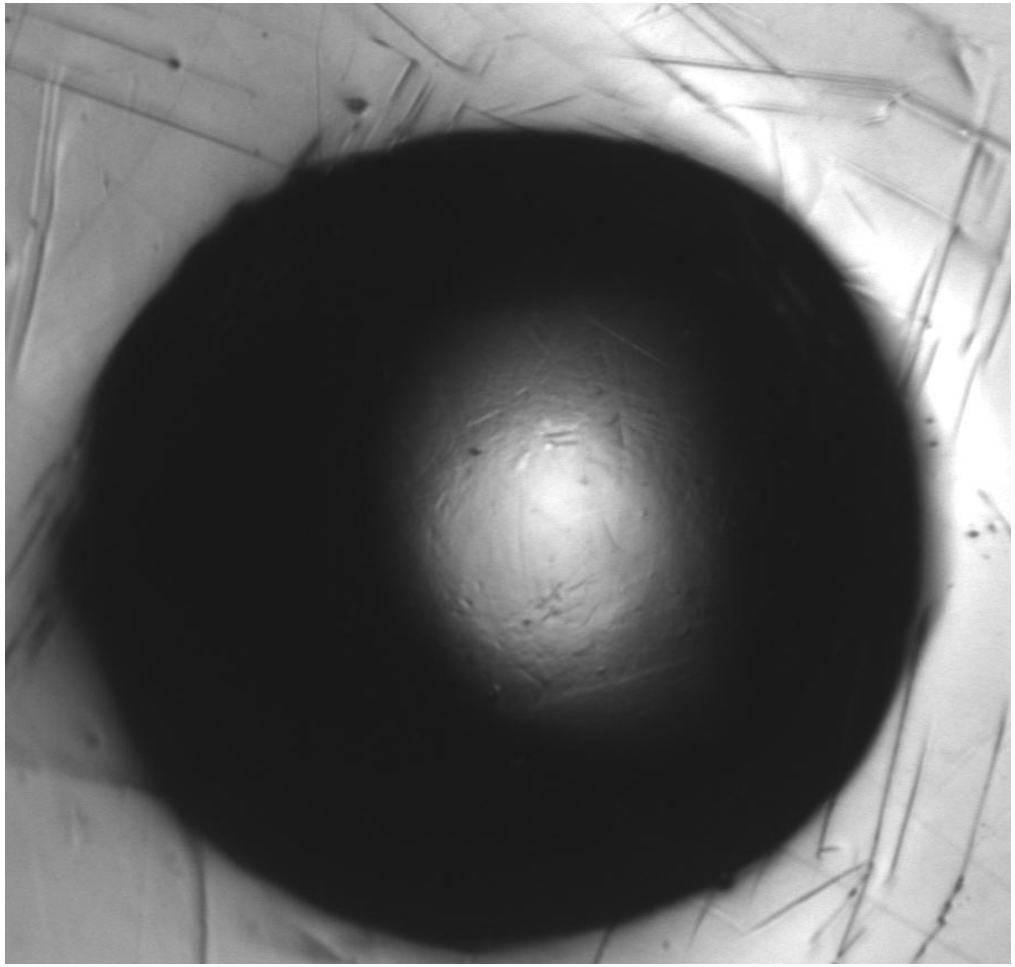

Application: ORNL Cast Re-(26-30) Cr wt% Alloy

- Initial multiple-partial unloadings for Young's modulus determination and followed by discrete loadings for post-yielding stress/strain data based on Tabor's equations.

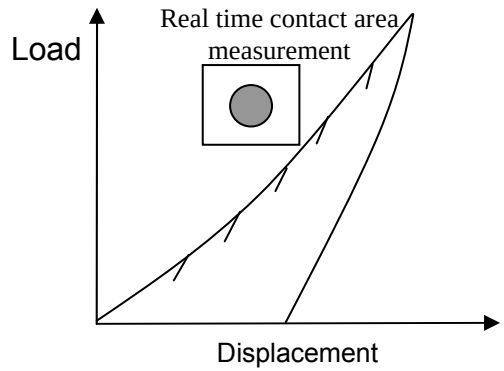

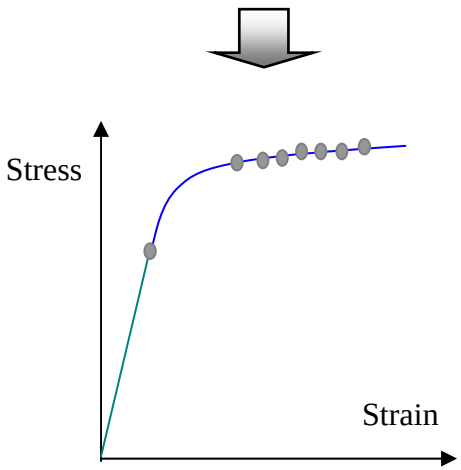

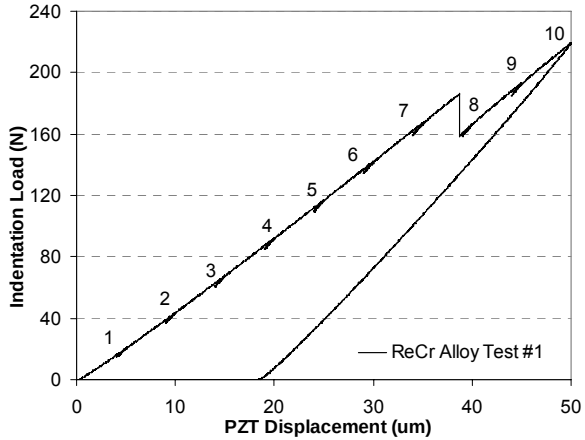

(a) Load-displacement curve

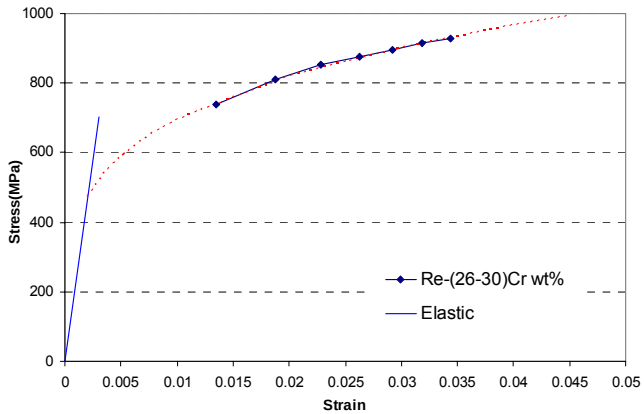

(c) Stress-strain curve, E=234GPa

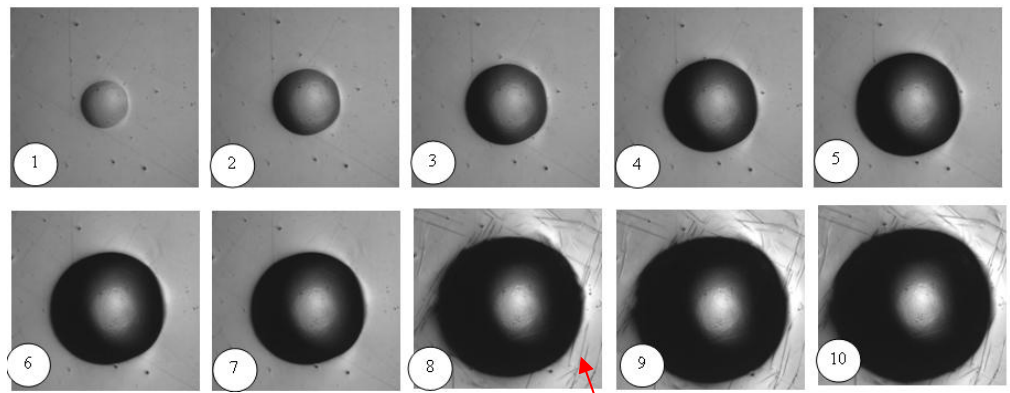

Showing formation of slip lines

(b) Visualization of indented surface, Field of view for each image: 395um x 377um

Gen III: Multi-Partial Unloading Indentation Technique
(A Load-Based Algorithm)

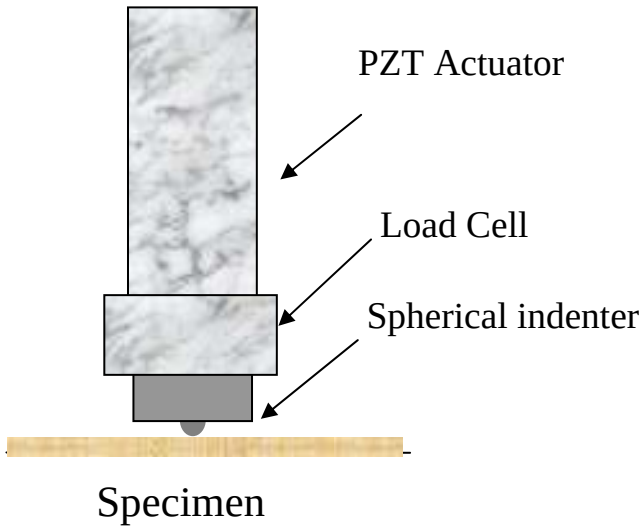

Load-depth sensing indentation system without imaging

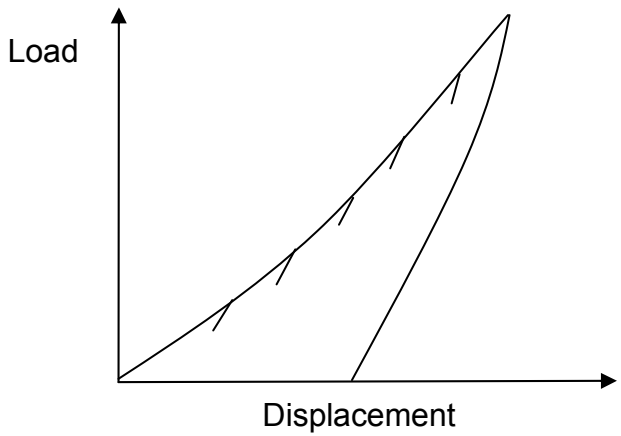

Multi-partial unloading indentation technique

Governing Equations

$$\frac{dh}{dp} = C \times \frac{1}{p^{1/3}} + C_s$$

$$C = \left(6RE_r^2\right)^{-1/3}$$

Applications:

- Young's modulus
- Stress-strain curve
- Indentation creep, fatigue

Potential:

Portable Indentation System

Load-Based vs. Contact Area - Based

- Spherical indentation, elastic

$$P = \frac{4}{3} \cdot \frac{\sqrt{R}}{k_0} h^{3/2}$$

P is the load, h is the depth, R indenter radius

$$k_0 = \frac{1}{E_r} = \frac{1-\upsilon^2}{E_d} + \frac{1-\upsilon^2}{E_i}$$

$$\frac{dP}{dh} = \frac{2}{\sqrt{\pi}} E_r \sqrt{A}$$

Base for load-depth sensing indentation

Under the assumption: $h = \frac{a^2}{R}$

$$\frac{dP}{dh} = (6RE_r^{\ 2})^{1/3} \cdot P^{1/3}$$

Load-Based Indentation

- Compliance form
  - No area, or contact region measurement

$$\frac{dP}{dh} = (6RE_r^{\ 2})^{1/3} \cdot P^{1/3}$$

$$\frac{dh}{dP} = (6RE_r^{\ 2})^{-1/3} \cdot P^{-1/3}$$

$$\frac{dh}{dP} = C \times \frac{1}{P^{1/3}}$$

Gen III: Multi-Partial Unloading Indentation Technique

$$\left.\frac{dh}{dp}\right|_1 = C \times \frac{1}{p_1^{1/3}} + C_s$$

$$\left.\frac{dh}{dp}\right|_2 = C \times \frac{1}{p_2^{1/3}} + C_s$$

Double-partial unloading

$$\left.\frac{dh}{dP}\right|_1 - \left.\frac{dh}{dP}\right|_2 = C \times \left(\frac{1}{p_1^{1/3}} - \frac{1}{p_2^{1/3}} \right)$$

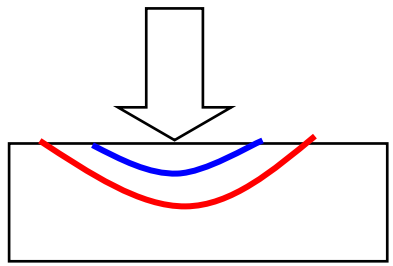

Multiple-partial unloading

$$\left(\frac{dh}{dp} \right) = C \times \left(\frac{1}{p^{1/3}} \right) + C_s$$

$$y = ax + b$$

$$x = \frac{1}{p^{1/3}}$$

$$y = \frac{dh}{dp}$$

$$a = C = \left(6RE_r^{\,2}\right)^{-1/3}$$

$$b = C_s$$

$$E = \frac{1 - v^2}{\frac{1}{E_r} - \frac{1 - v_0^2}{E_0}}$$

Gen III: Validation Tests

- IN 783 (E = 177GPa), measured E=169 GPa

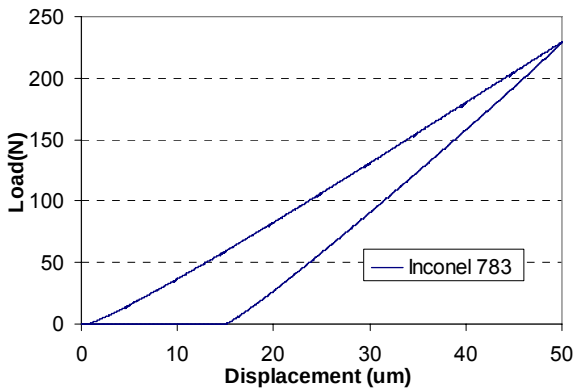

Load-depth curve

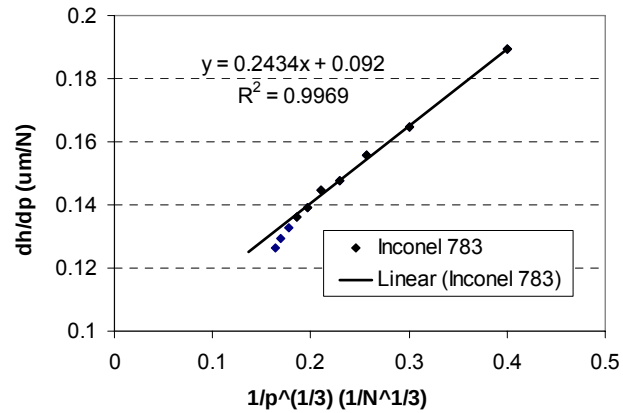

Compliance curve

- Al 7075-T6 (E= 71 GPa), measured E = 67 GPa

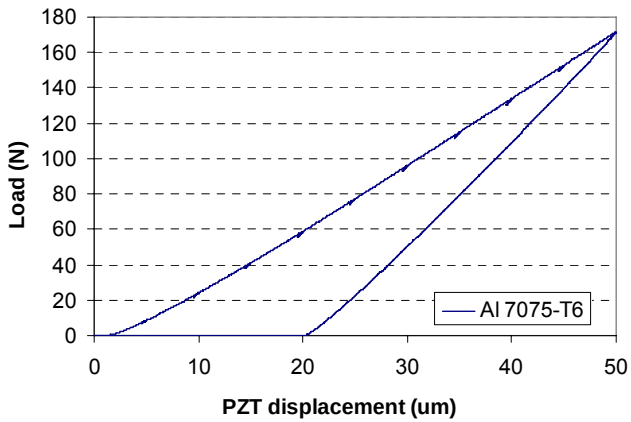

Load-depth curve

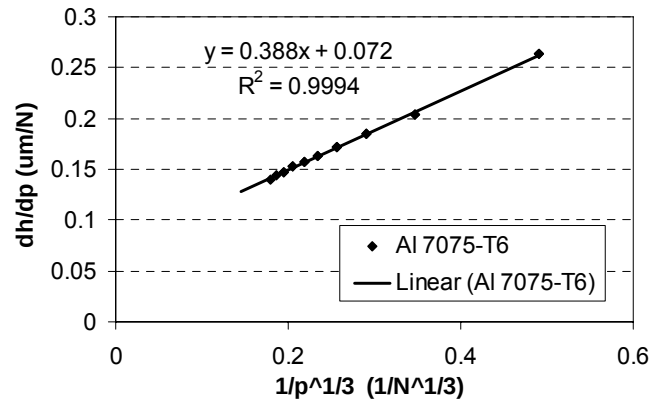

Compliance curve

Gen III: Benefits

- Designed for TBC/Bond Coat specimen
  - Measurement of surface stiffness responses as a means to correlate the evolution of the microstructural changes of the TBC bond coat/substrate subjected to high temperature thermal cycles.
  - Can also be correlated to the damping effect
  - No surface preparation is needed
  - Simple and has the potential to develop a portable unit for in-situ field testing
- Controllable influence zone
  - As load increases, the influence zone increases.
  - The response is contributed from different region of the multi-layered material

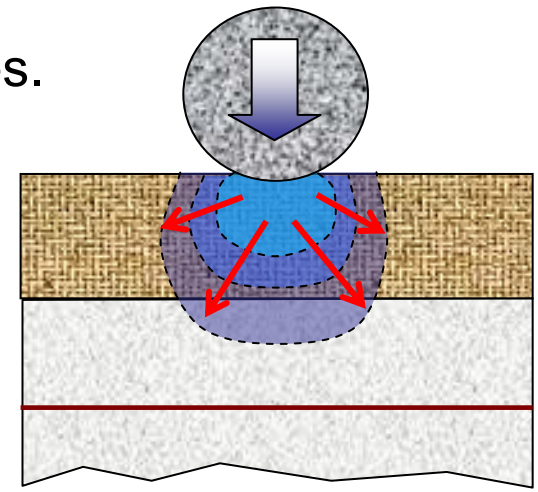

$$\frac{dh}{dp} = C \times \frac{1}{p^{1/3}} + C_s$$

Gen III: Multi-Partial Unloading Indentation Technique
(A Load-Based Algorithm)

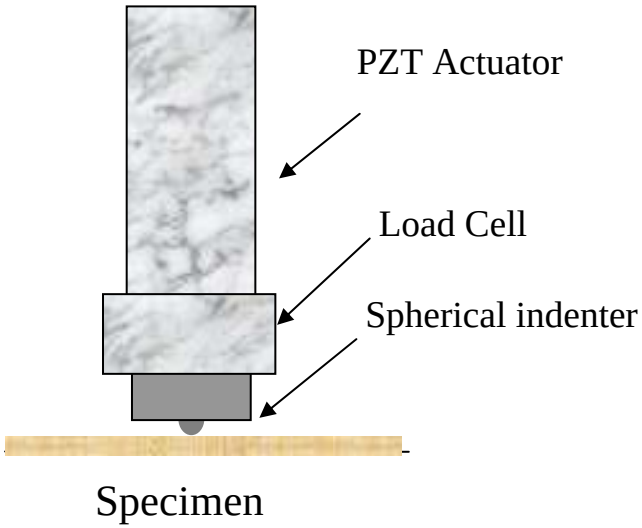

Load-depth sensing indentation system without imaging

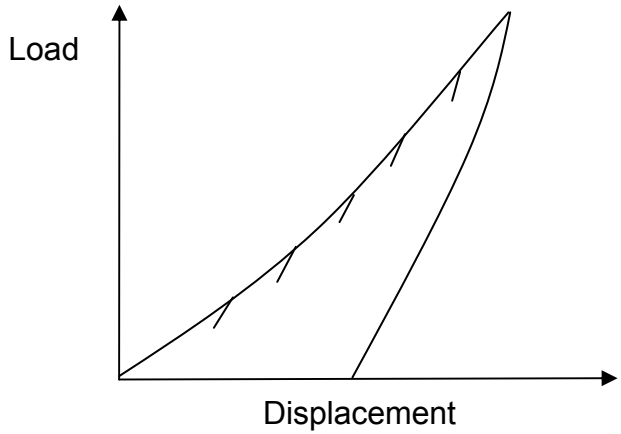

Multi-partial unloading indentation technique

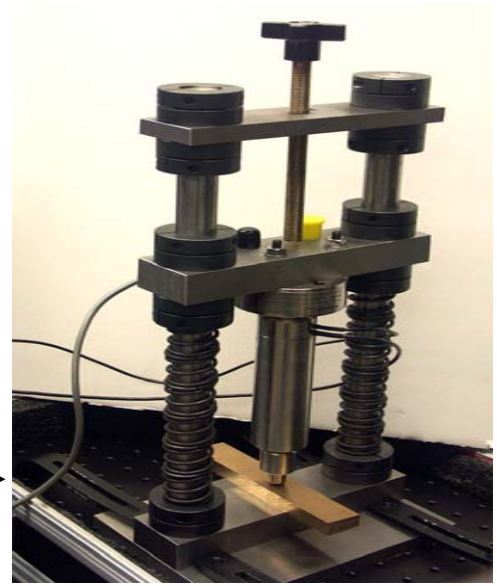

Table-top Unit

Applications:

- Young's modulus
- Stress-strain curve
- Indentation creep, fatigue

Potential:

Portable Indentation System

Governing Equations

$$\frac{dh}{dp} = C \times \frac{1}{p^{1/3}} + C_s$$

$$C = \left(6RE_r^2\right)^{-1/3}$$

Portable Micro-Indentation System

- A prototype portable micro-indentation system
- Software Development
  - Establish initial condition
  - Setup testing parameters
  - Acquire load-depth information
  - Use load-based algorithm for data processing
  - Indentation Results

Table-Top Micro-Indentation Unit

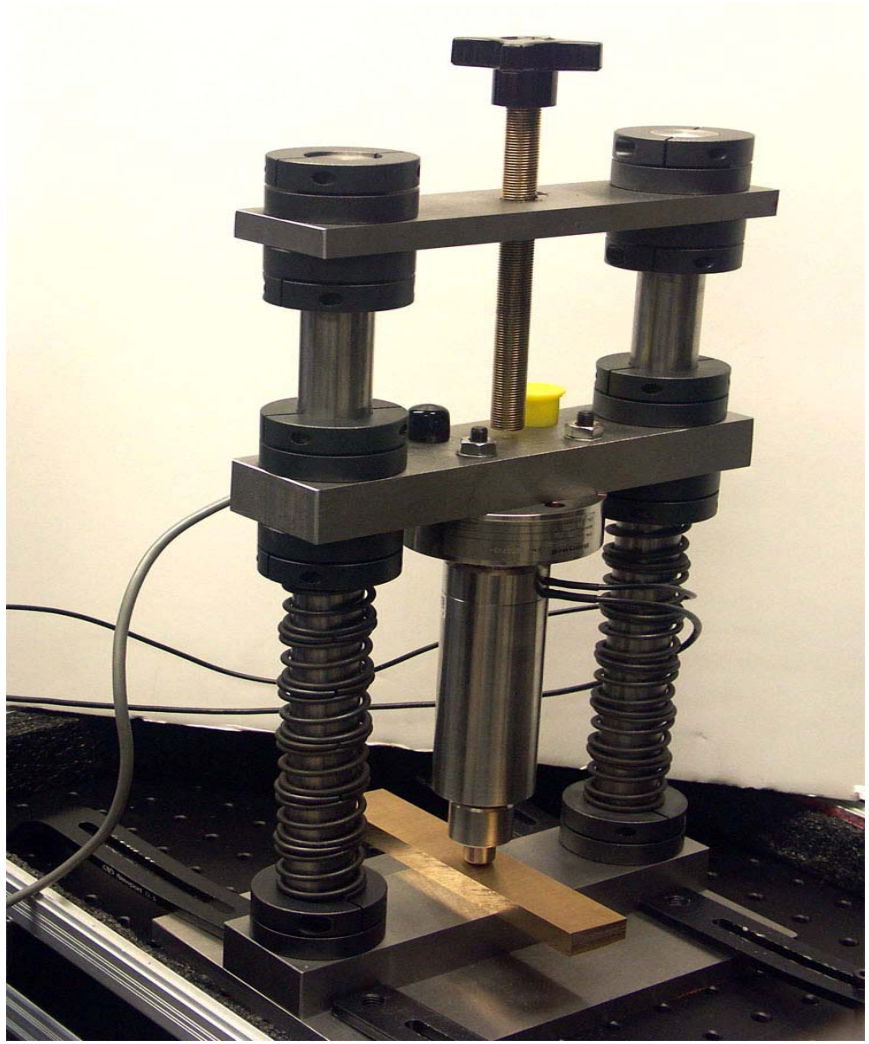

Portable Micro-Indentation Unit

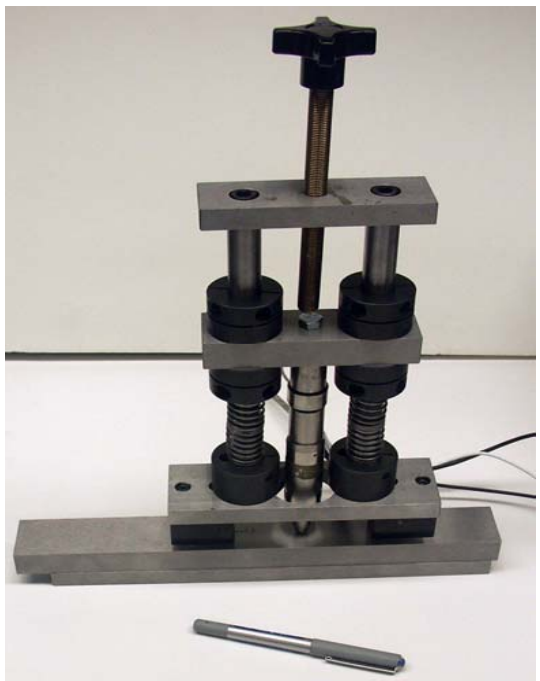

Establish Initial Condition

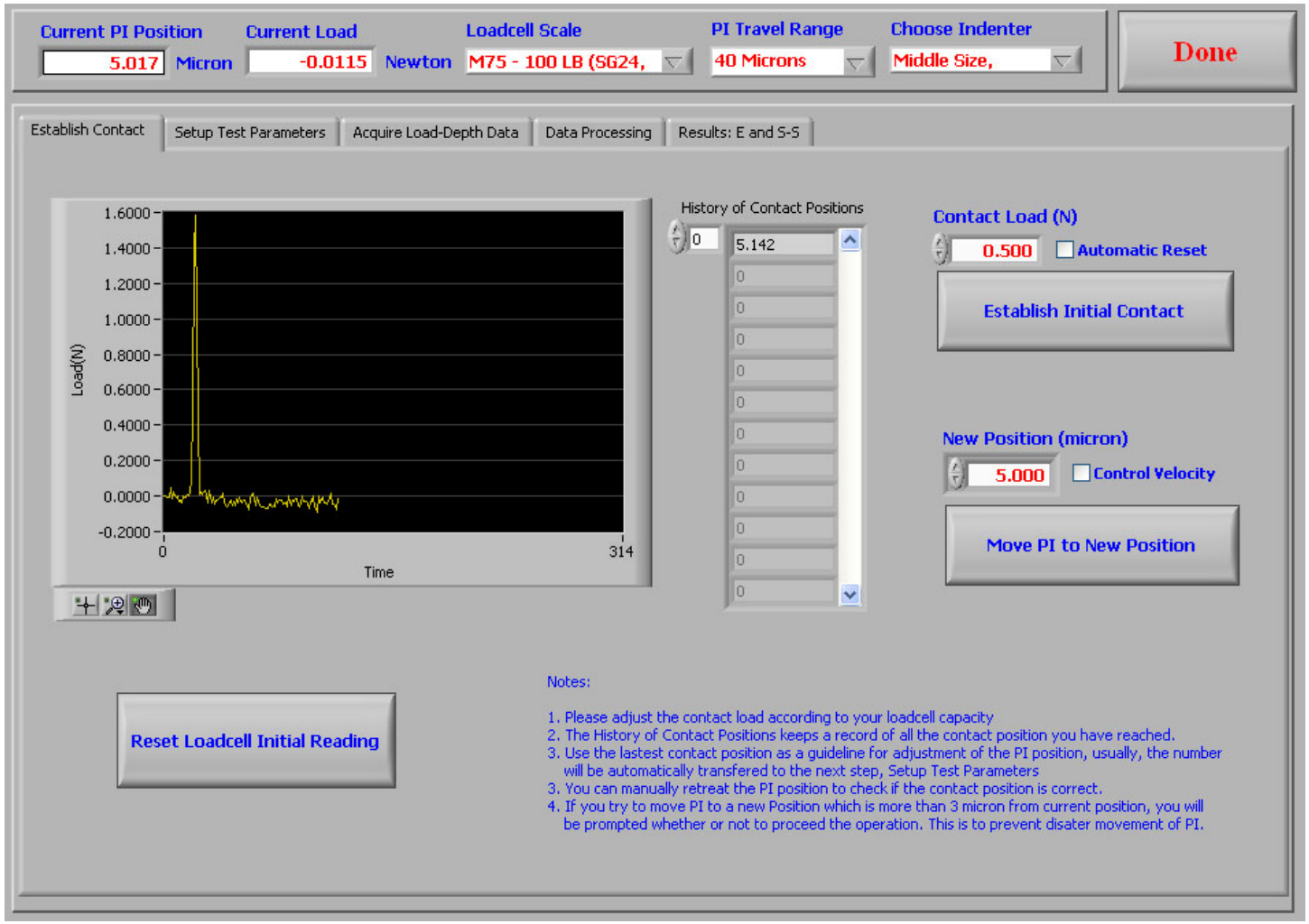

Setup Testing Parameters

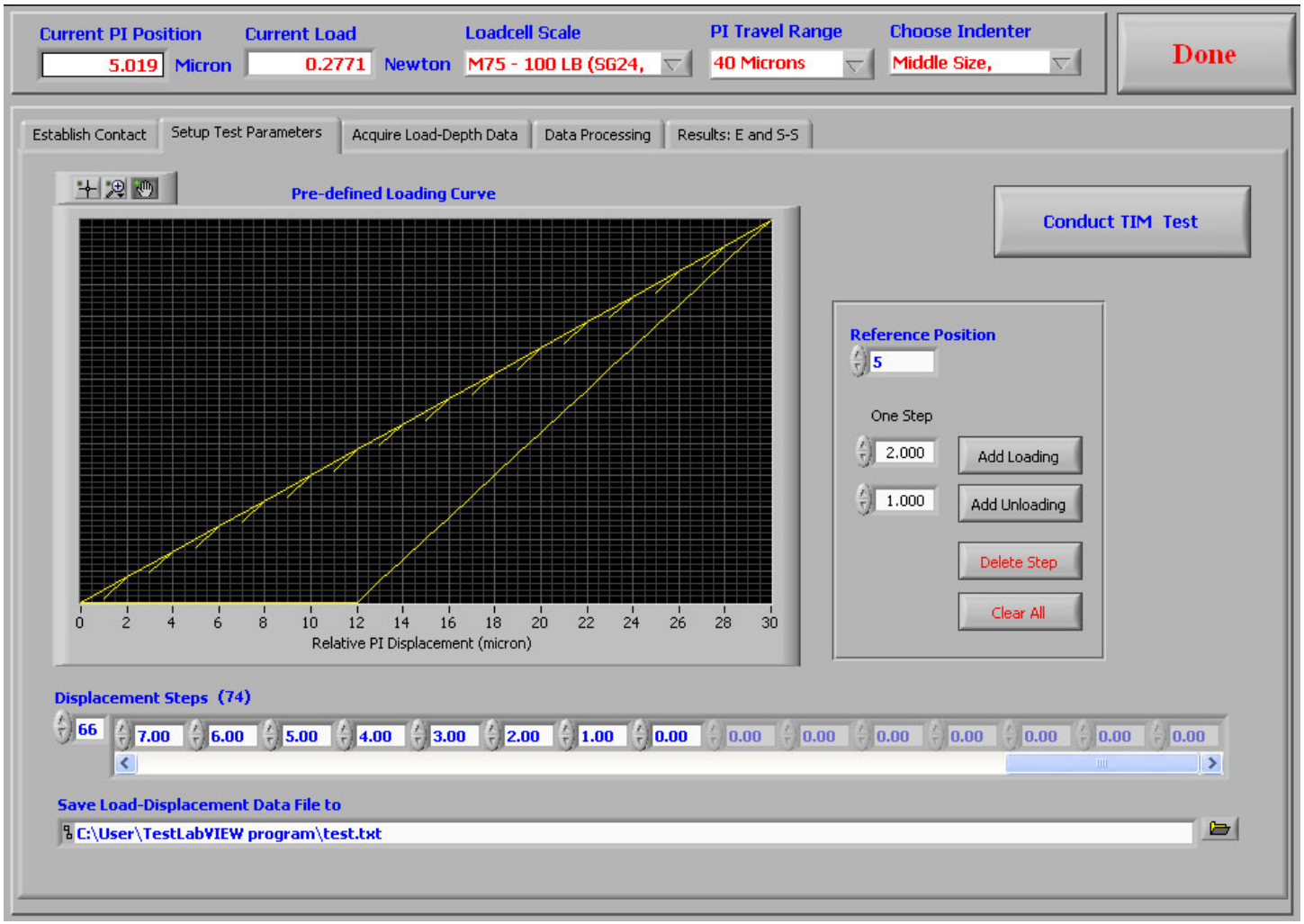

Acquire Load-Depth Information

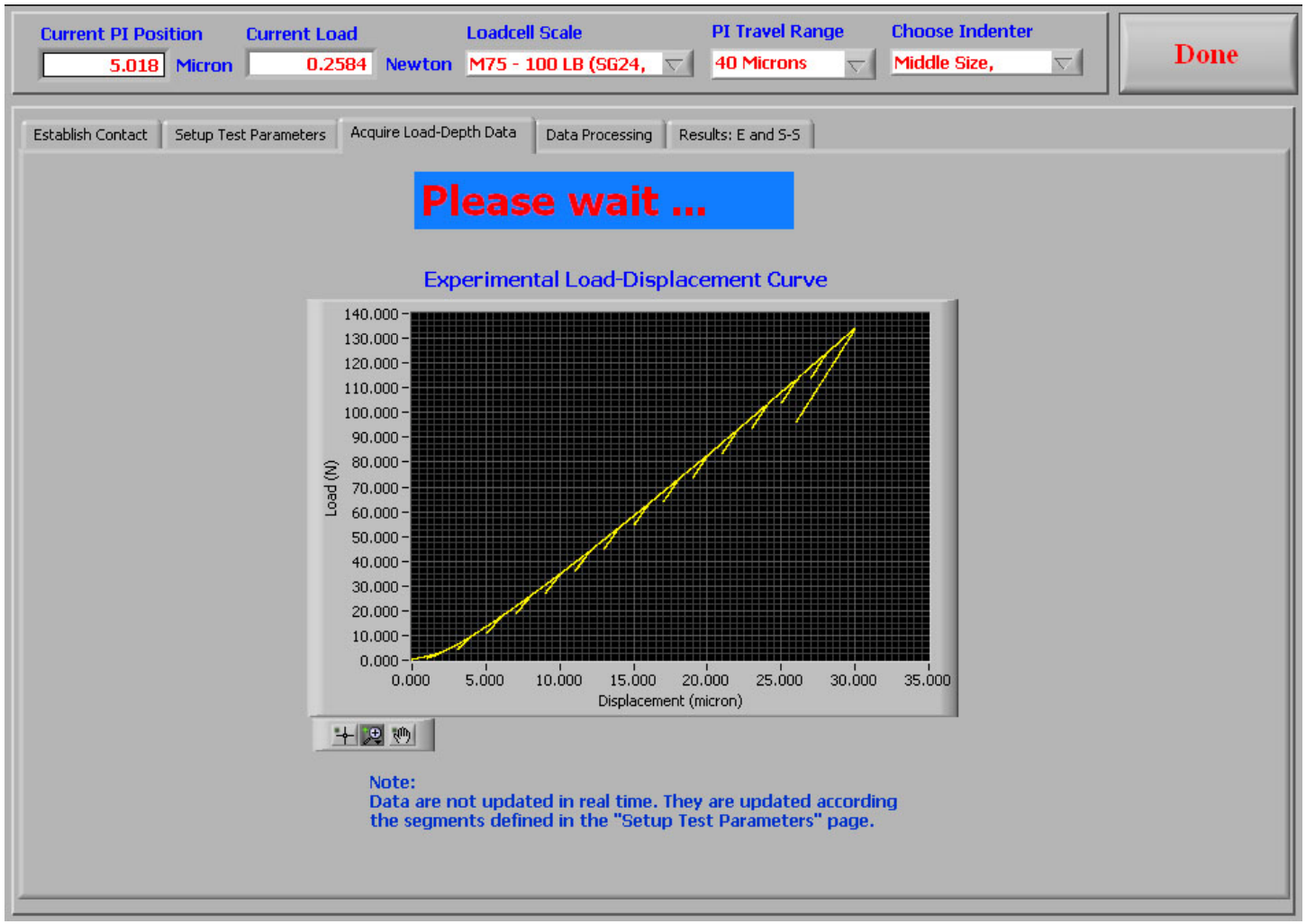

Use Load-based Algorithm for Data processing

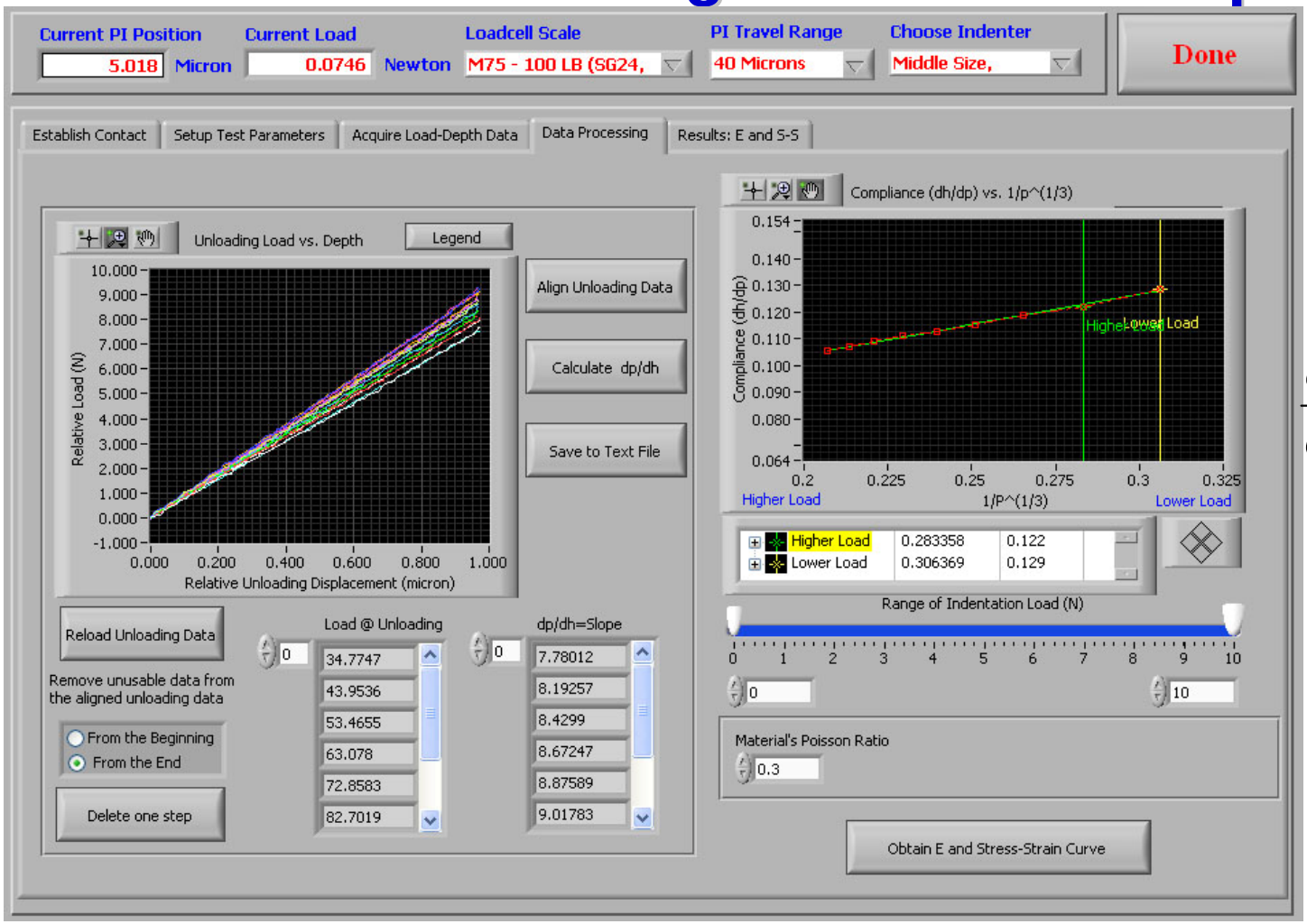

$$\frac{dh}{dp} = C \times \frac{1}{p^{1/3}} + C_s$$

Indentation Results

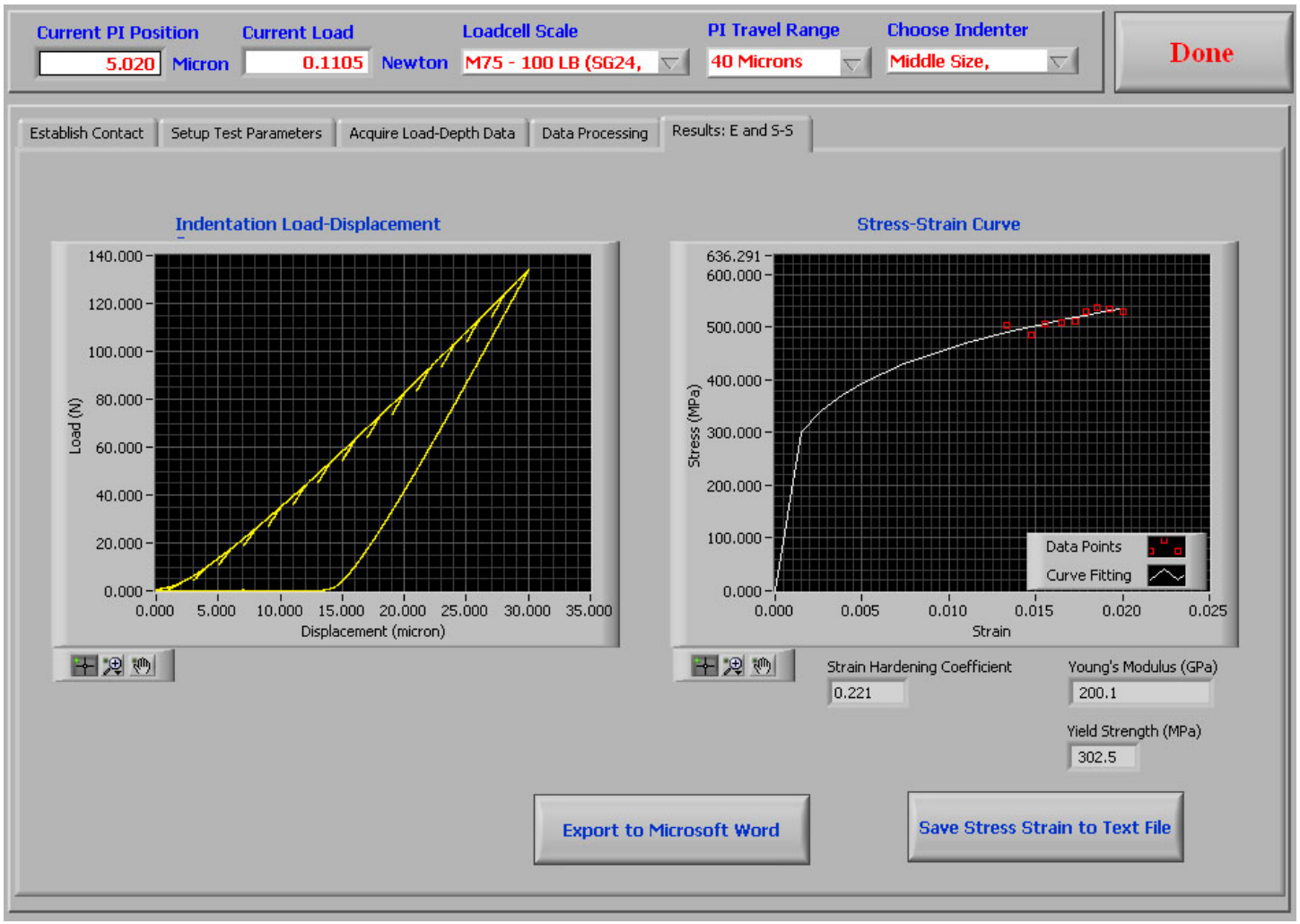

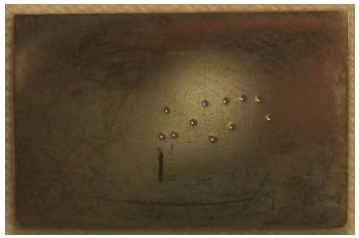

Mo+Nano MgAl2O4 (MCP)

Mo+Nano MgO

#697 (Mo+MgAl2O4)

Mo+Nano MgAl2O4

#678 (Mo+MgAl2O4)

Mo+Nano MgAl2O4

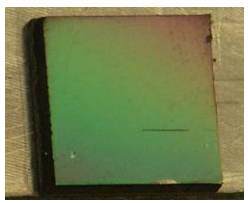

Fuel Cell Interconnect Coating

Metallic Glass

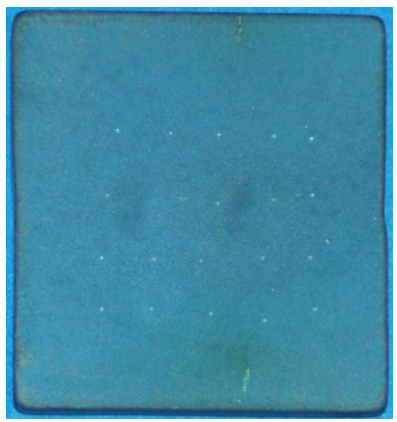

Bond Coat

TBC

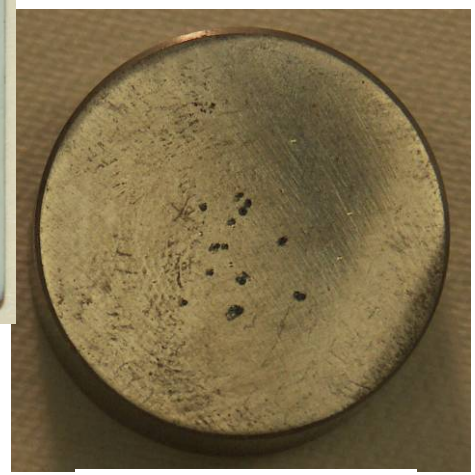

4140 steel

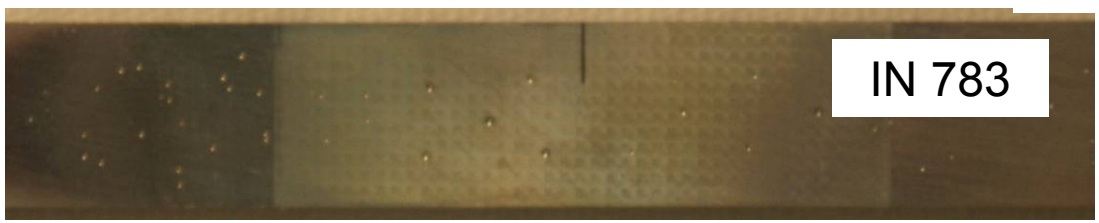

1" (25.4mm)

Resolution and Accuracy

- PZT actuator accuracy: 4 nm
- Loading accuracy: 0.05 N
- Indenter size: 1/16” (diameter, or R = 793 μm)

(For micro-indentation on Mo alloys and other high strength alloys)

- Typical loading range: 40 N to 200 N
- Typical contact diameter: ~ 200μm (100 to 300 μm)
- Estimated max. indentation depth: ~ 6 μm (4 to 12 μm)

(For micro-indentation on TBC specimens)

- Typical loading range: 60 N to 200 N
- Typical contact diameter: ~ 200 μm (150 to 280 μm)
- Estimated max. indentation depth: ~ 6 μm (4 to 10 μm)

Portable Indentation System Design & Applications

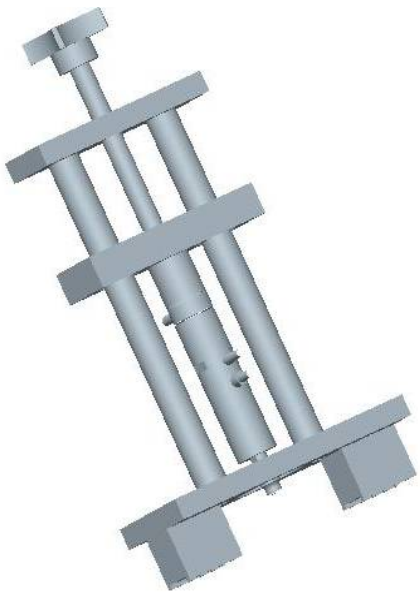

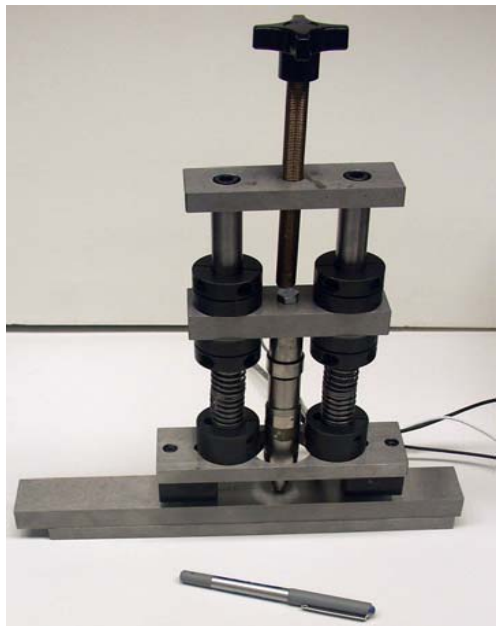

Portable micro-indentation system with electromagnetic or v-notch mount

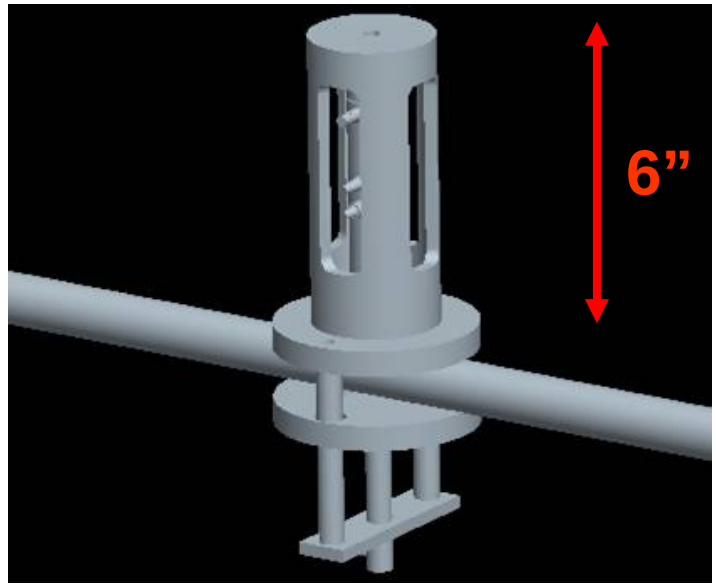

Latest portable micro-indentation system suitable for curved / flat surfaces

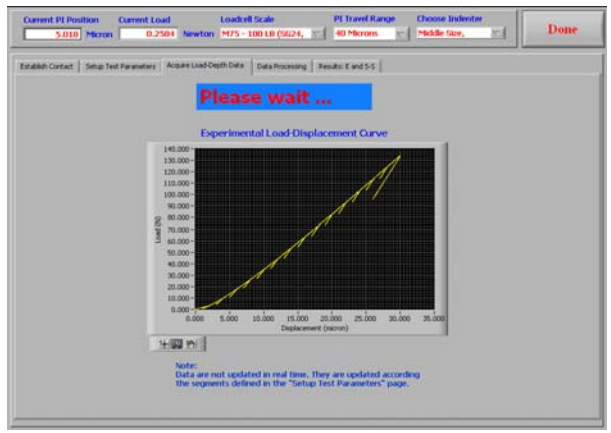

Software for both units

Portable Micro-Indentation Test at Different Orientation On Curved/Flat Surfaces

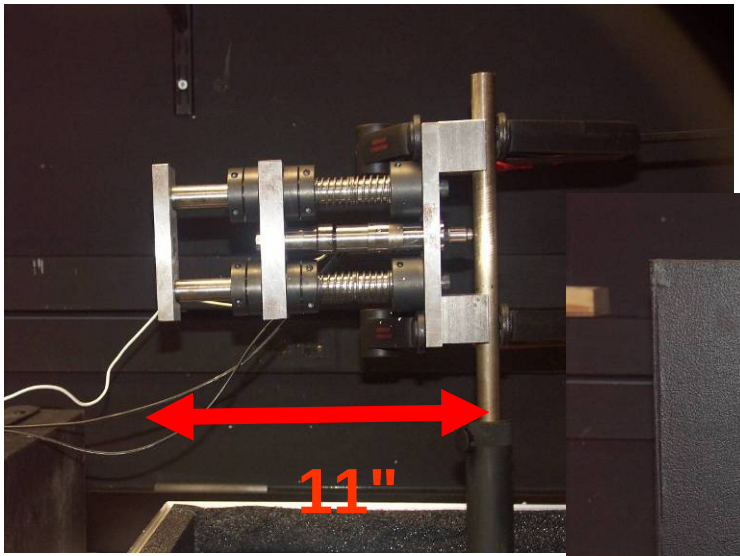

Vertical Position for curved surface

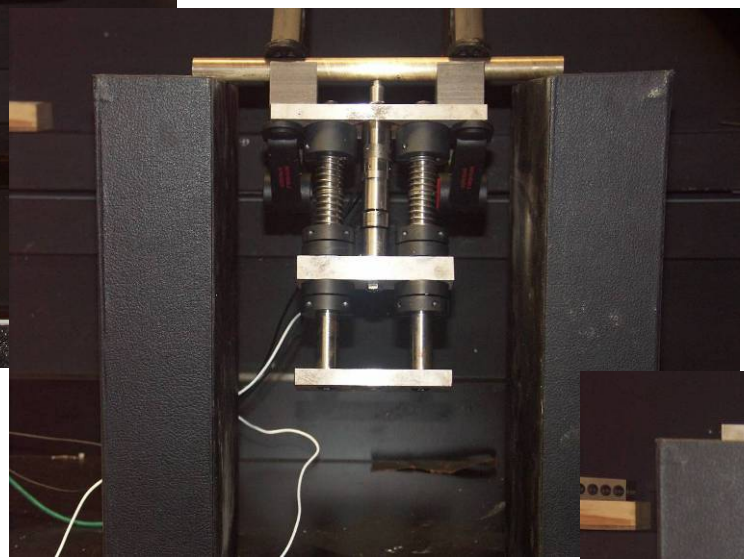

Upside down position for curved surface

Upside down Position for flat surface

Validation Tests

Flat Surface

Test	***Bronze 932***	***Aluminum 6061***	***01 Tool Steel***
Number	*GPa*	*GPa*	*GPa*
Book Value	**103 -124**	**68 - 71**	**190 - 210**
1	109.98	68.23	207.92
2	113.74	68.57	209.78
3	113.98	68.14	210.01
4	109.90	68.43	204.75
5	111.99	70.51	211.66
6	115.45	69.07	209.78
7	119.02	68.40	210.48
8	114.06	77.15	212.37
9	121.97	73.40	215.03
10	124.38	67.77	199.94
Average	**115.45**	**69.97**	**209.17**
Standard Deviation	**4.88**	**3.03**	**4.22**

Curved Surface

Test	***Bronze 932***	***01 Tool Steel***
Number	*GPa*	*GPa*
Diameter	3/4"	3/4"
Book Value	**103 -124**	**190 - 210**
1	95.54	209.19
2	96.99	211.59
3	107.50	188.23
4	103.96	197.05
5	117.80	197.83
6	107.15	202.24
7	96.69	187.51
8	100.06	184.33
Average	**103.21**	**197.25**
Standard Deviation	**7.54**	**10.12**

High-Temperature Micro-Indentation Tests (Preliminary)

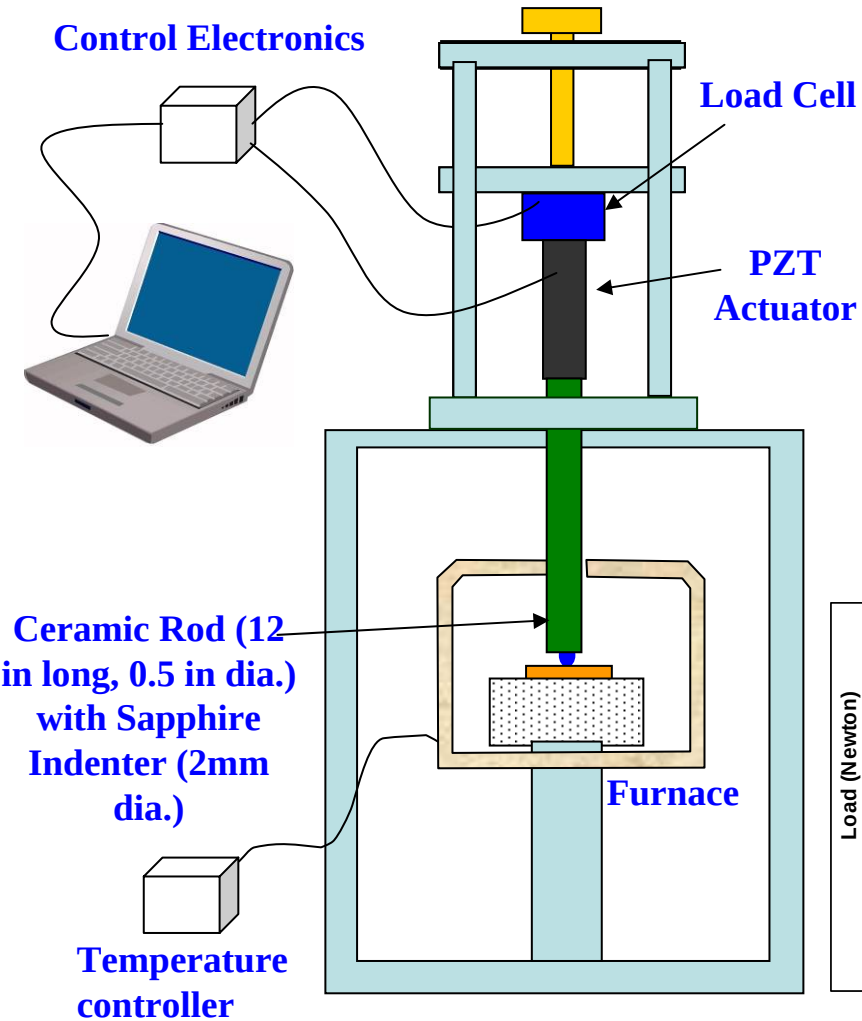

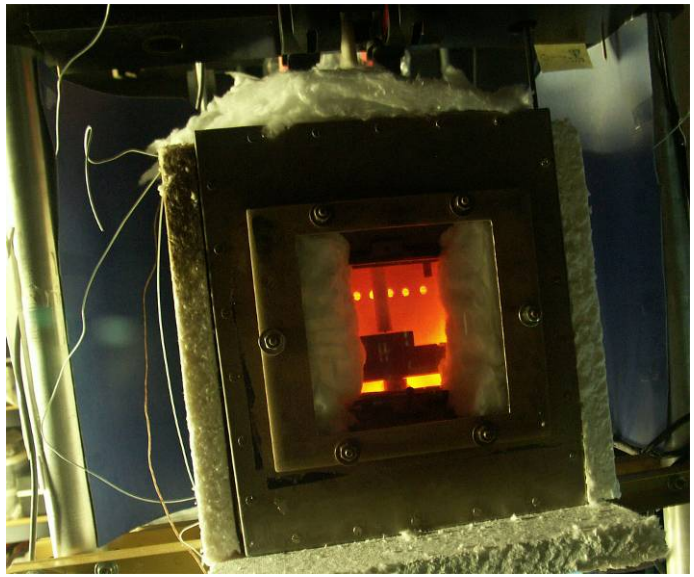

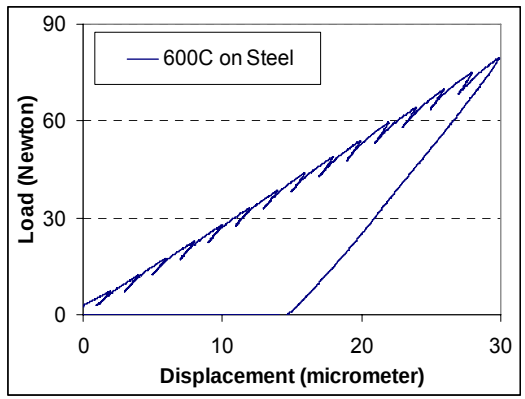

Steel at 600C
(Measured E~160GPa)

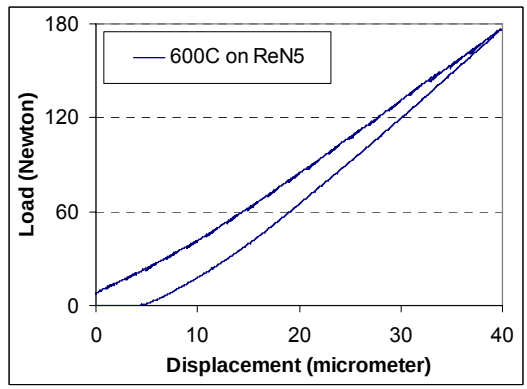

ReN5 at 600C
(Measured E~70GPa)

Materials Matrix

(Alloys received from M.P. Brady and J. H. Schneibel, ORNL)

#678, Mo-3.4wt%$MgAl_2O_4$: 1800°C/4hr/3ksi/Vacuum, Mo powder 2-8μm, $MgAl_2O_4$, 1-5μm

#696, Mo-3.0wt%$MgAl_2O_4$: 1800°C/1hr/3ksi/Vacuum, Mo powder 2-8μm, $MgAl_2O_4$, 1-5μm

#695, Mo only : 1800°C/1hr/3ksi/Vacuum, Mo powder 2-8μm

#697, Mo-6.0wt%$MgAl_2O_4$: 1800°C/1hr/3ksi/Vacuum, Mo powder 2-8μm, $MgAl_2O_4$, 1-5μm

#698, Mo-3wt%MgO : 1800°C/1hr/3ksi/Vacuum, Mo powder 2-8μm, MgO, 1-5μm

Cast Re-(26-30) Cr wt% nominal

(Powder mix prepared at WVU using Ultrasound Mixing Technique and sent to ORNL for vacuum hot-pressed)

Mo-5.0wt%$MgAl_2O_4$: 1800°C/0.5hr/3ksi/Vacuum

Mo-5wt%MgO : 1800ºC/1.0hr/3ksi/Vacuum

Mo-5.0wt%TiO_2 : 1700°C/0.5hr/3ksi/Vacuum

(Powder mix prepared using Hosakawa Mechano Chemical Bonding processing technique from Hosokawa, then vacuum hot-pressed)

Mo-2.5wt%$MgAl_2O_4$ (Before MCB process): 1800°C/0.5hr/3ksi/Vacuum

Summary: Young's Modulus Measurement

Material	Young's modulus (GPa)
Cast Re-(26-30) Cr wt%	234
#678, Mo-3.4wt%$MgAl_2O_4$	229
#696, Mo-3.0wt%$MgAl_2O_4$	200
#697, Mo-6.0wt%$MgAl_2O_4$	192 (Tensile test : 189)
#698, Mo-3wt%MgO	211
Mo-MgO (WVU)	254
Mo-MgAl2O4 (WVU)	202
Mo-TiO2 (WVU)	226

(Averaged value from five indentation tests, typical)

Anaytical results show a small tensile zone on the surface next to the indentation zone

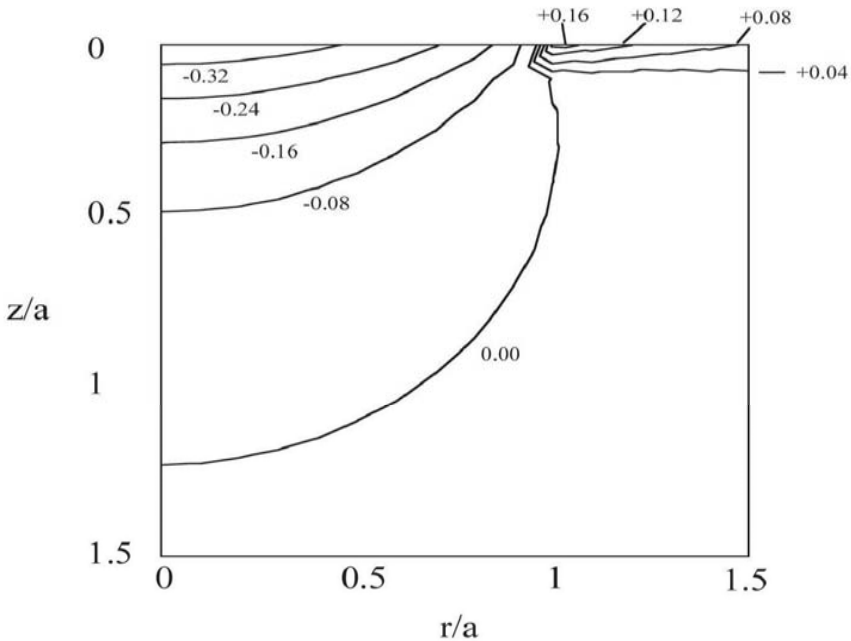

Figure 2: Contours of the most positive principal stress normalized to the peak Hertzian pressure. Elastically similar contact. Poisson's ratio ν = 0.24. After Warren et al. [6].

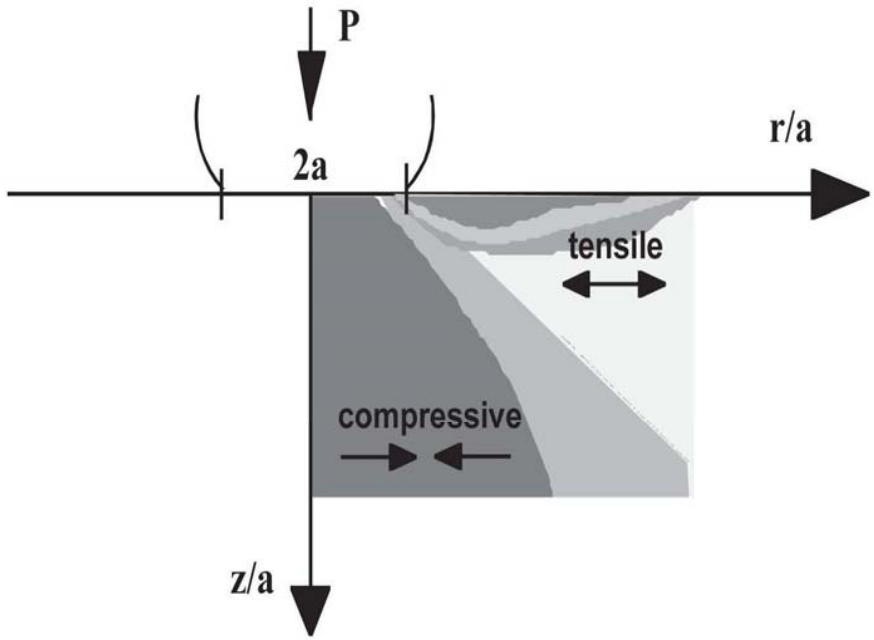

Figure 3. Tensile and compressive, σ_{rr} field in a substrate under a Hertzian load.
[Figura 3: Região sob tensão radial e compressiva, σ_{rr}, devido uma carga Hertziana.]

(From: A. Franco Jr., S. G. Roberts, Ceramica 50 (2004) 94-108)

Verification by finite element simulation (WVU)

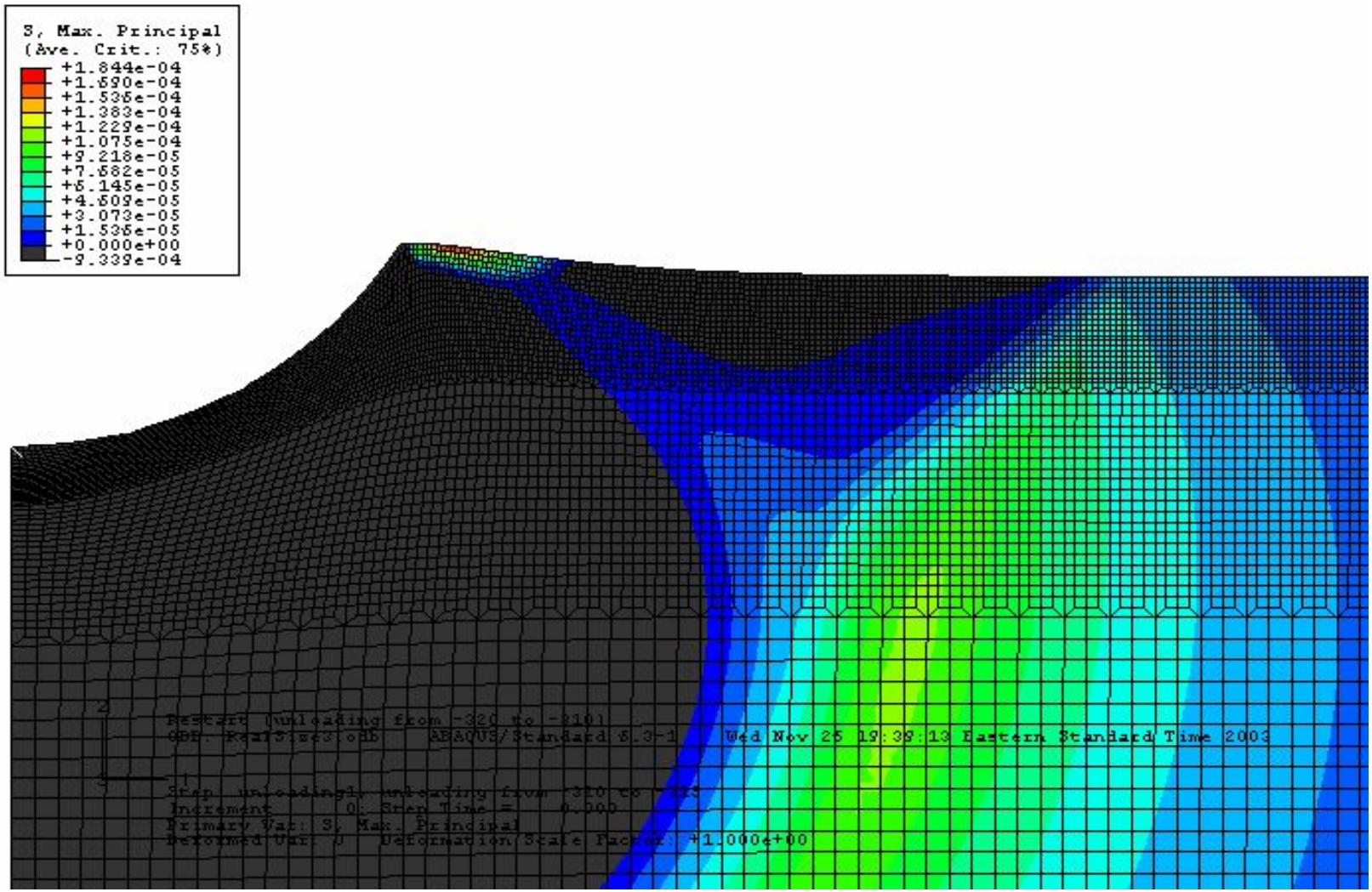

Material surface condition evaluation of Mo alloys with spinel particles

SEM observation at 2000x

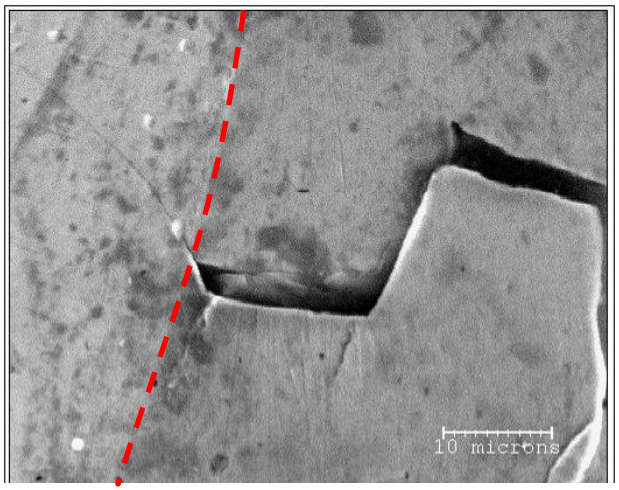

#695, brittle, indentation load 1500N, cracks are observed

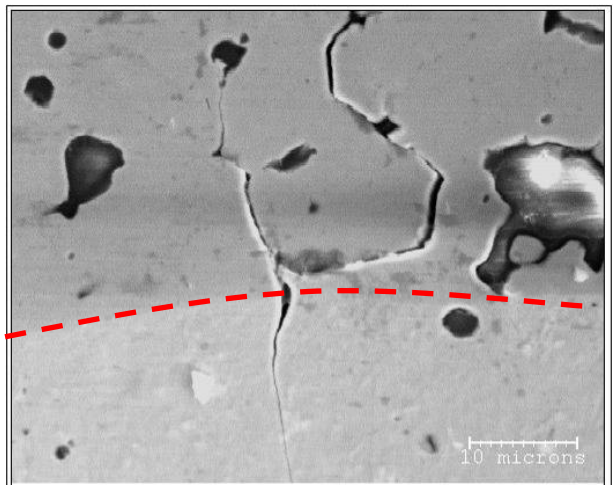

#697, brittle, indentation load 1000N, cracks are observed

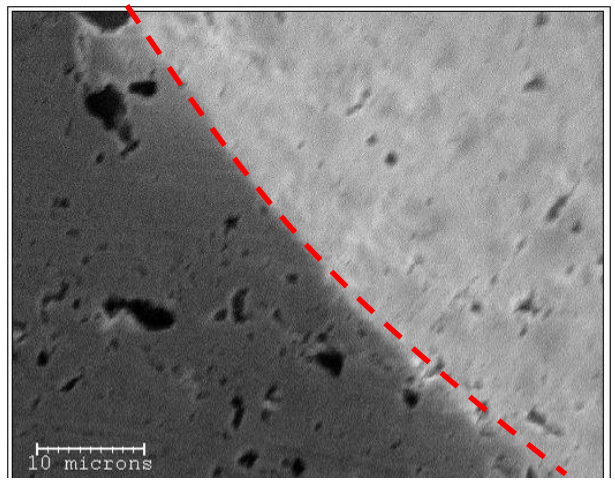

#678, Ductile, indentation load 2000N, no cracks were observed

Note: Dashed lines are indent boundaries

#698, Mo-3wt%MgO

- 400N indentation, cracking

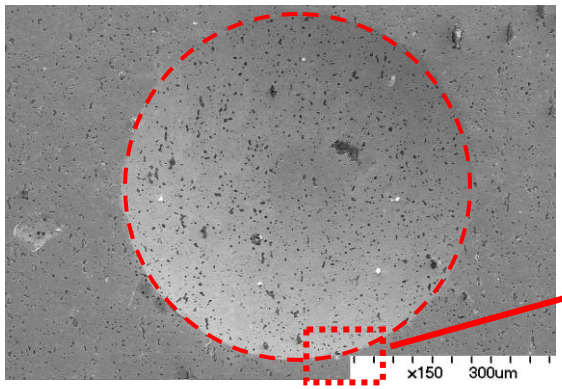

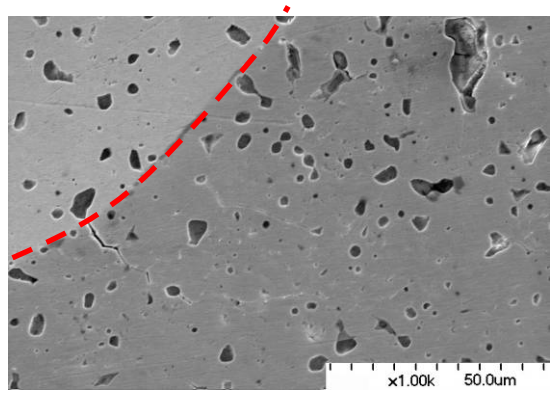

- 1000N indentation, cracking

1000N indentation with 1.6mm WC indenter

(Image size: 321μm×240μm)

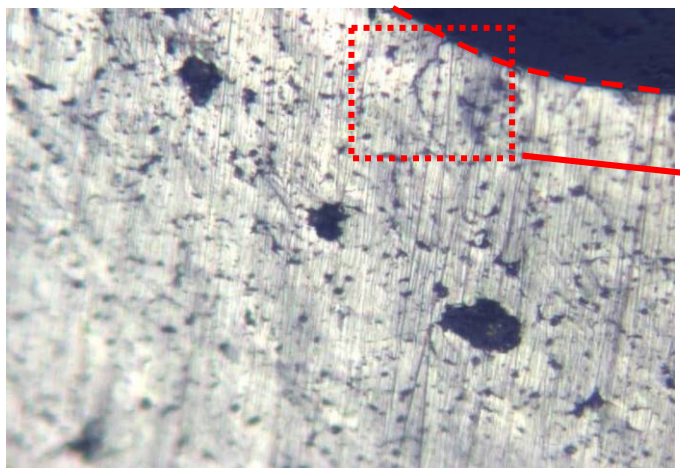

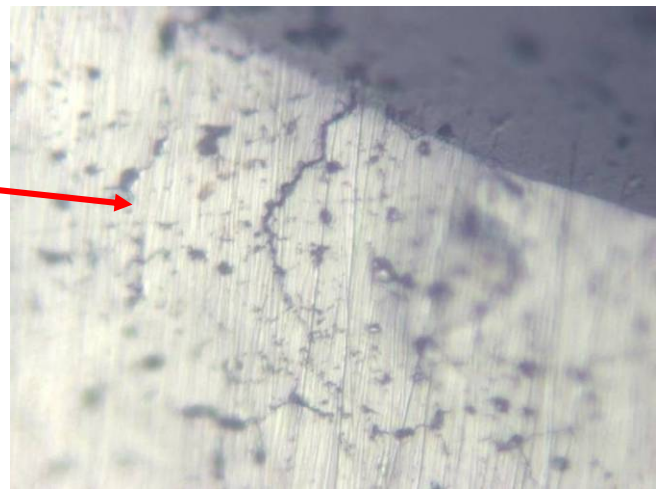

#696, Mo-3.0wt%$MgAl_2O_4$

- 400N indentation, cracking

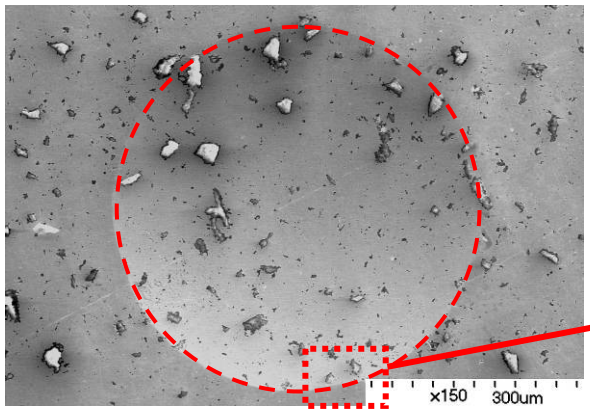

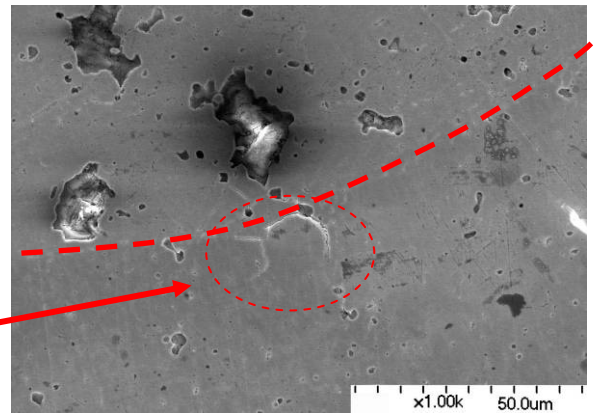

- 1000N indentation, cracking

1000N indentation with 1.6mm WC indenter

(Image size: 321μm×240μm)

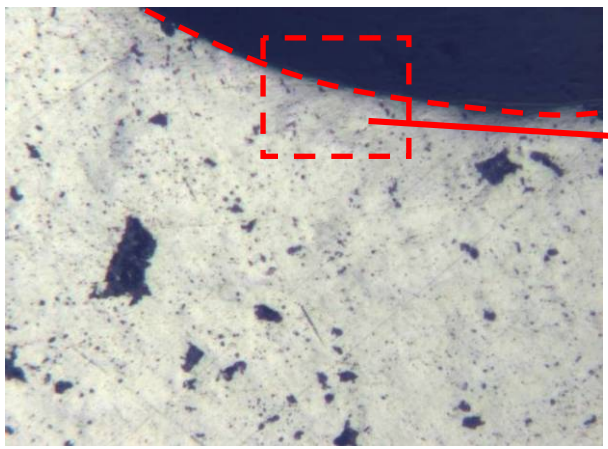

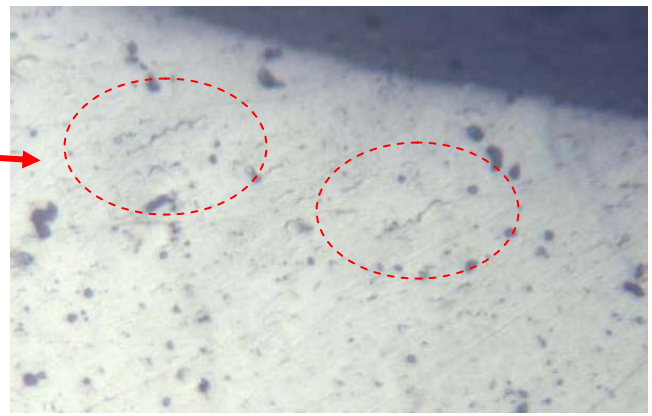

(WVU $MgO_{0.05}Mo_{0.95}$, $TiO_{2\ 0.05}Mo_{0.95}$, $MgAl_2O_{4\ 0.05}Mo_{0.95}$ Powder Mixes)

(1) 95 g of Mo powder (65 nm nominal) was mixed in ethyl alcohol and sonicated for 10 minutes using a high intensity sonicator (VC 600) in the presence of Argon.

(2) Then 5 g of MgO or TiO_2 or $MgAl_2O_4$ powder (20 nm nominal) was added slowly to the Mo solution with continuous sonication. The total mixture was sonicated for 1 hour in Argon atmosphere.

(3) The solution was kept at room temperature in Argon-filled glove box to let the ethanol evaporate for 24 hours. The remaining alcohol was removed by drying the product in vacuum.

(4) The dried powder was kept in Argon filled glove box and packed in a bottle in the presence of Argon.

Mo-TiO_2 (WVU)

- 400N indentation, cracking

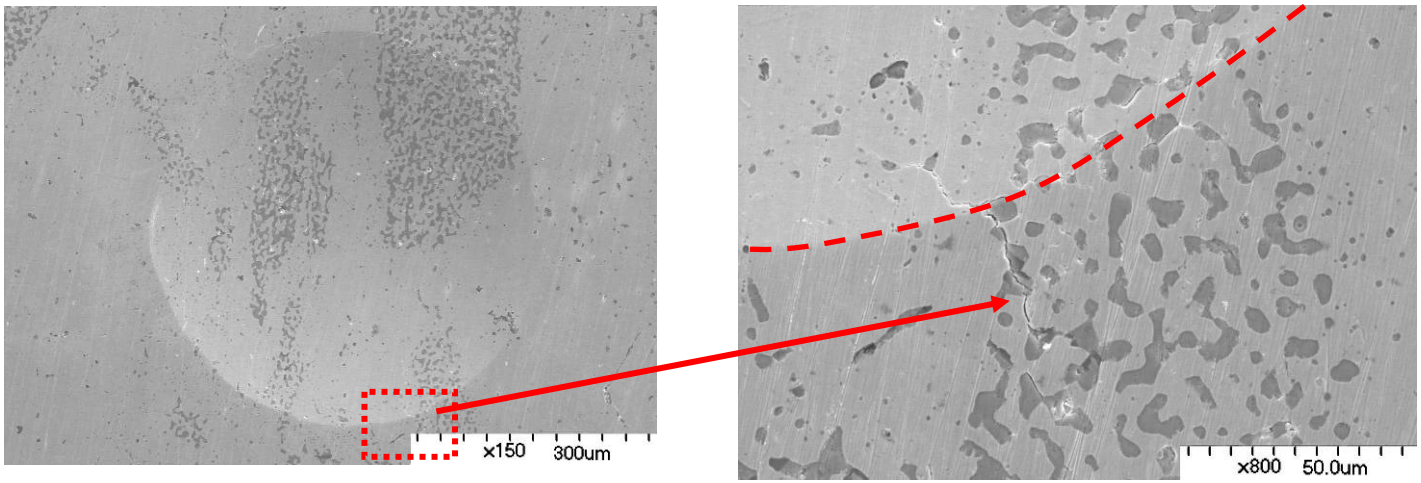

- Vickers hardness

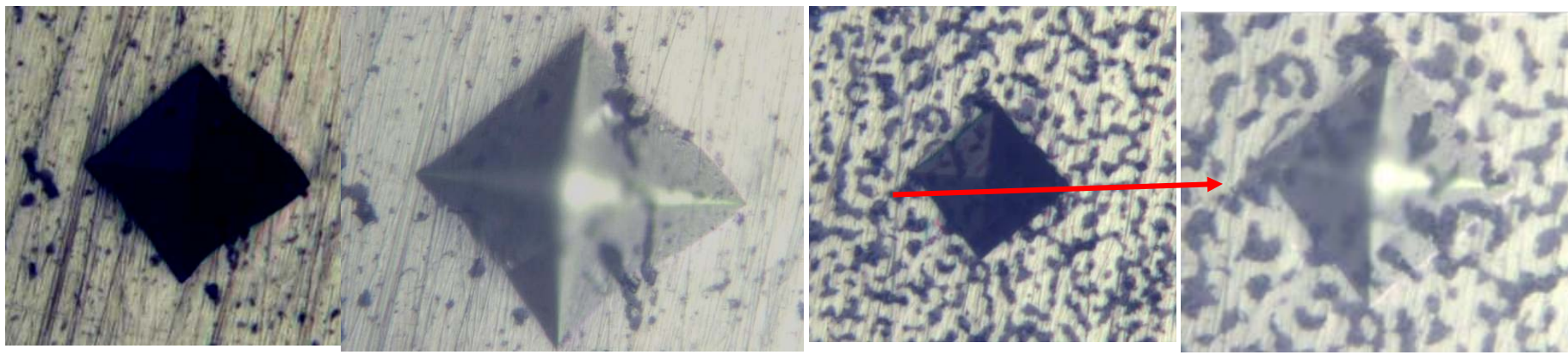

223HV, 1kg, 30s

353HV, 1kg, 30s

Mo-MgO (WVU)

- 400N indentation, cracking

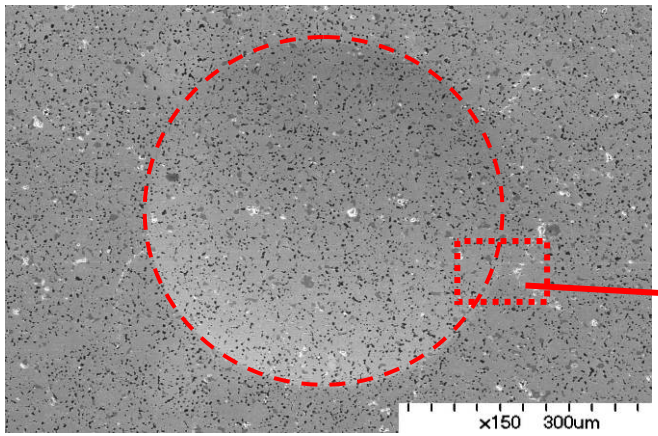

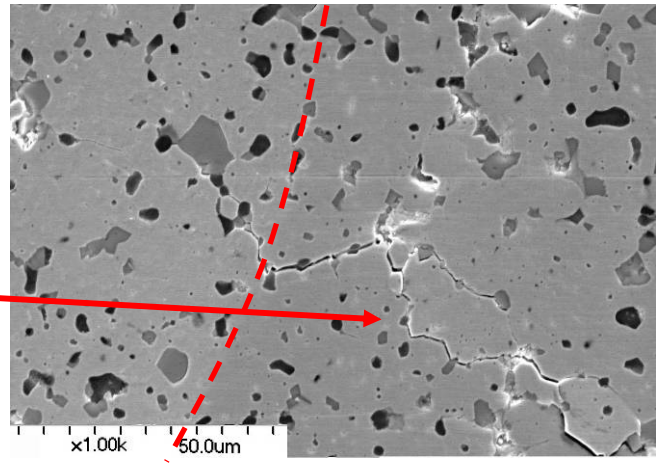

- Vickers hardness, 249HV, 1kg, 30s

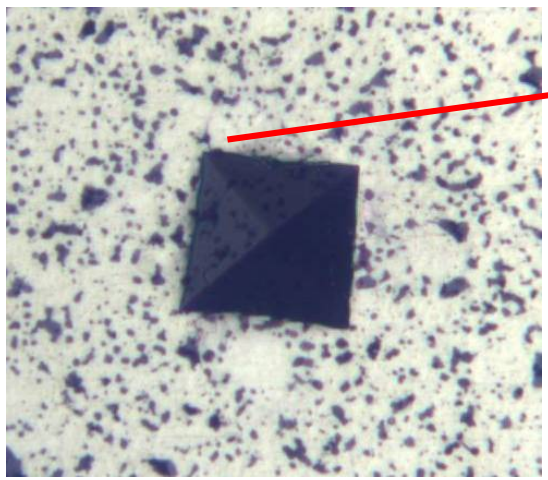

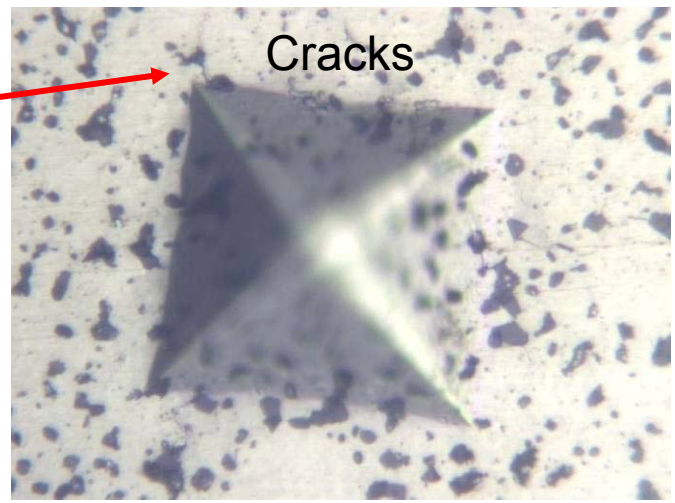

Mo-$MgAl_2O_4$ (WVU)

- 400N indentation, no cracks in MgAl2O4 uniformly distributed region

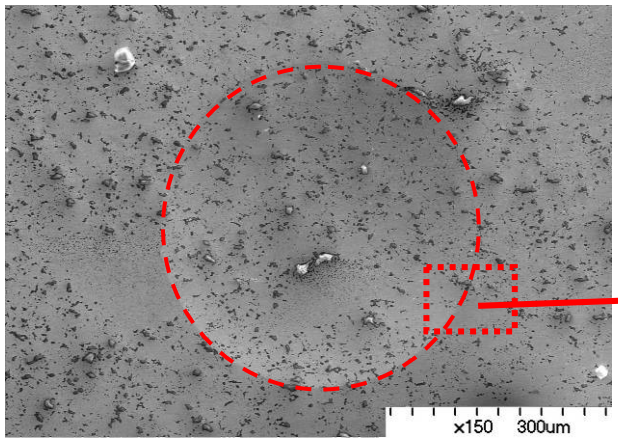

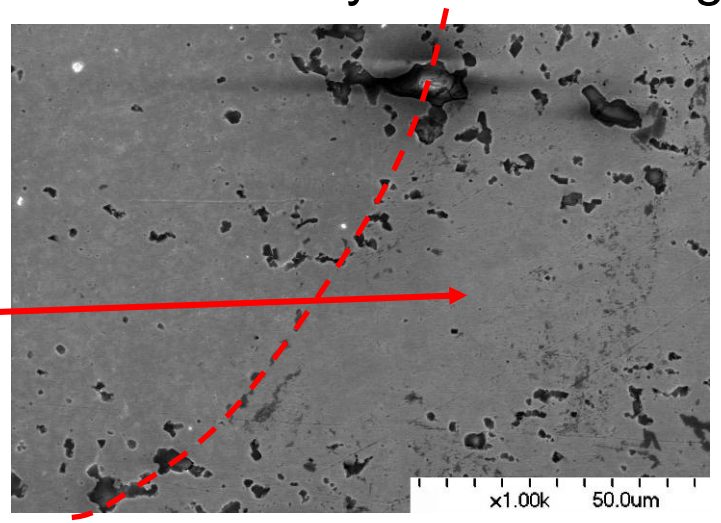

- Vickers hardness (plastic flow observed)

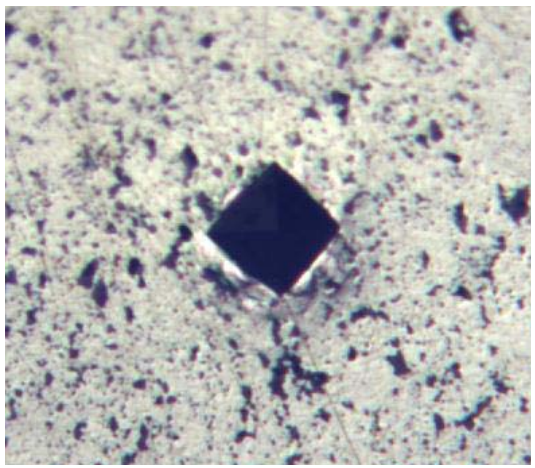

276HV, 1kg, 30s

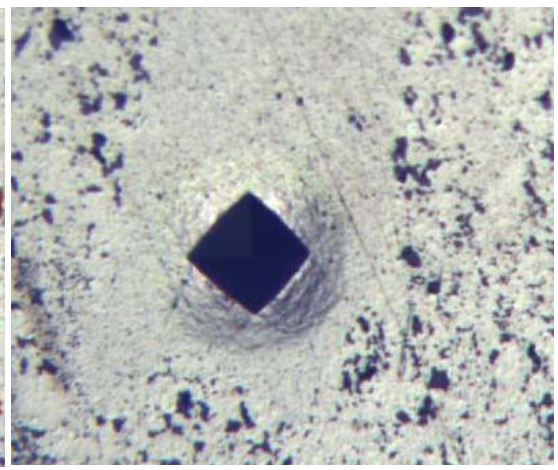

344HV, 1kg, 30s

Hosokawa Mechano Chemical Bonding Technology

The powder mixture introduced into the internal cavity of the equipment is subjected to a centrifugal force which transports them to the inner wall of the rotating chamber. The powder mixture is then subjected to additional compression and shear mechanical forces as they rotate and pass through a gap between the chamber wall and what is referred to as a press head.

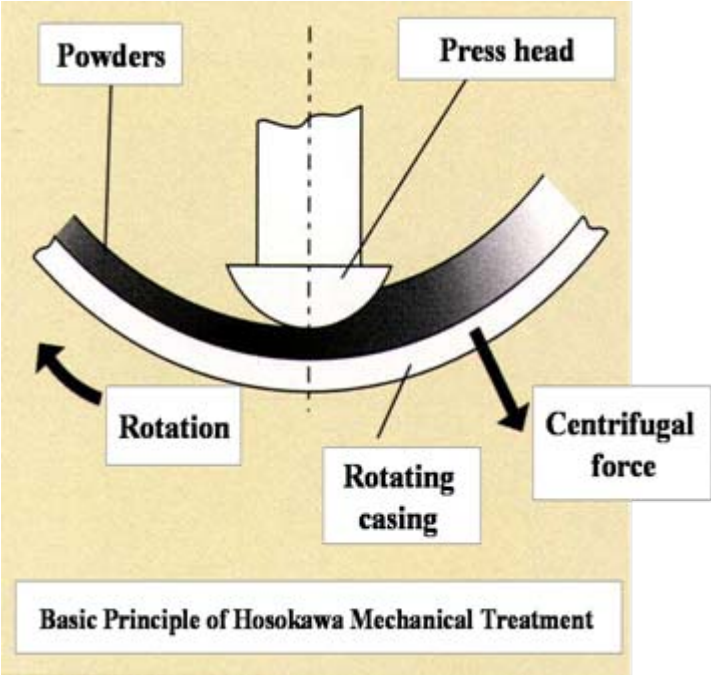

This results in the smaller particles being dispersed and bonded onto the surfaces of larger base particles without using any binders. This technique can also be applied to improve particle sphericity and for precision mixing of nano and submicron powders.

Powder Mixing Using Mechano-Chemical Bonding Technique

450 gram of Mo-$MgAl_2O_4$ powder mixes (97.5wt% Mo (size: 2 to 6 μm) and 2.5wt% $MgAl_2O_4$ (size: 30 nm)) were processed by Hosokawa's Mechano-Chemical Bonding technique

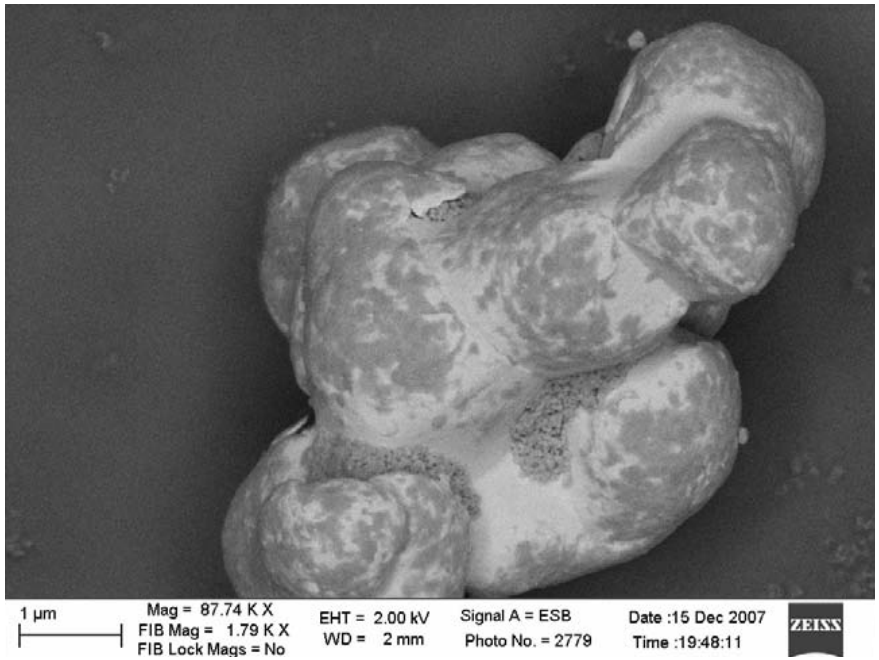

SEM image: $MgAl_2O_4$ coverage: brighter areas have less $MgAl_2O_4$.

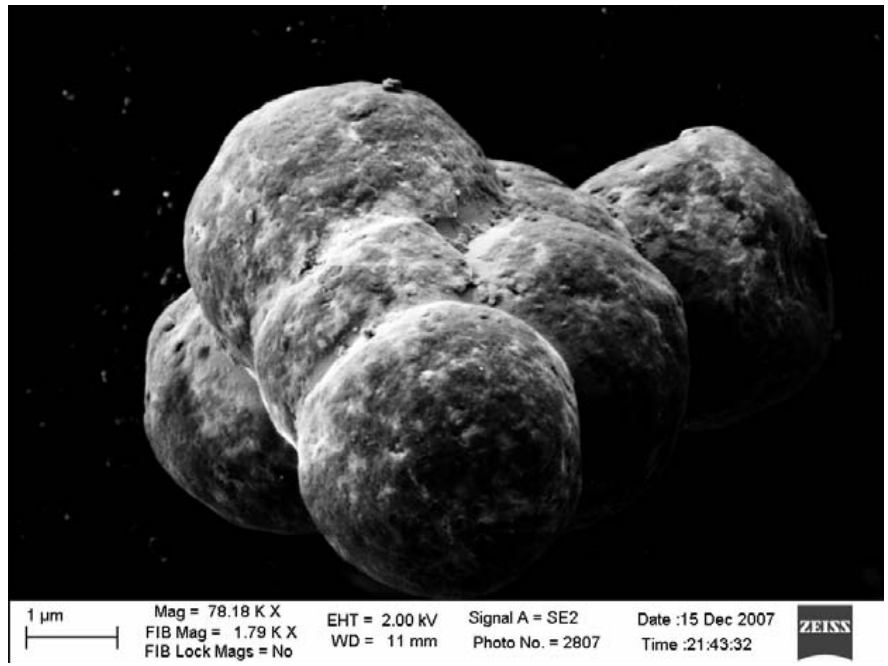

$MgAl_2O_4$ coverage

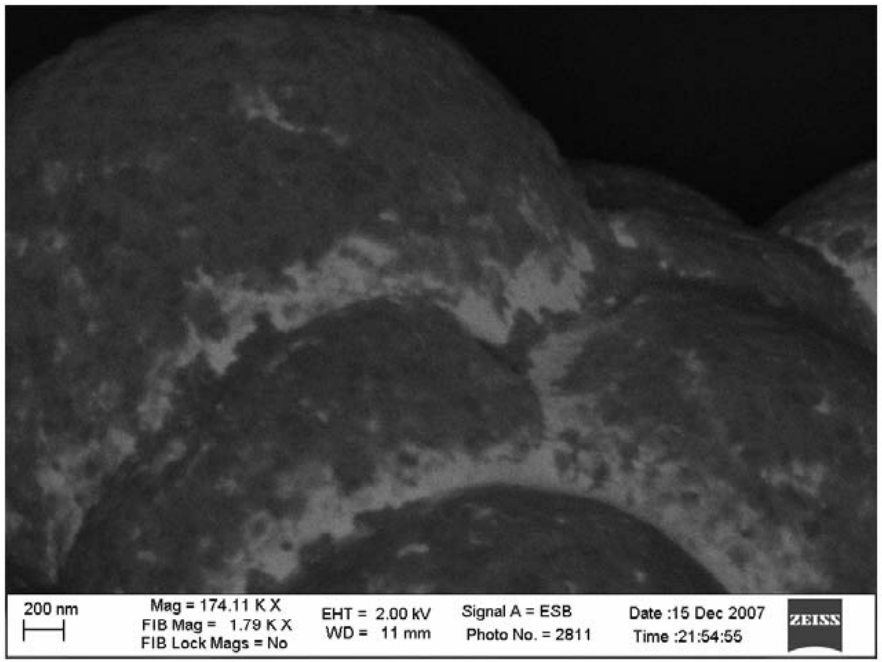

More SEM image: $MgAl_2O_4$ coverage
(Energy-selected backscattering detector)

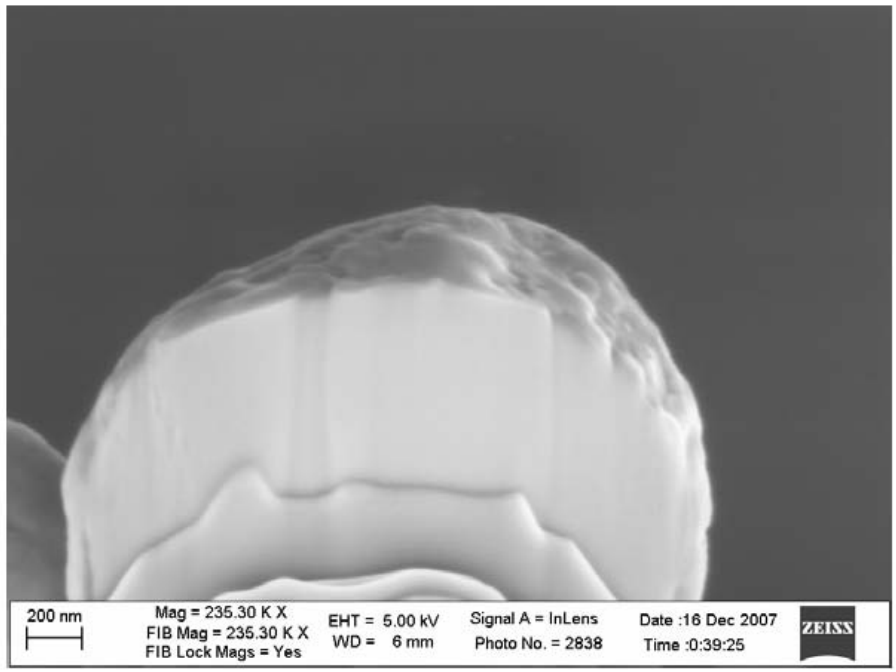

SEM image (Inlens detector)
Mo particle is cut by FIB

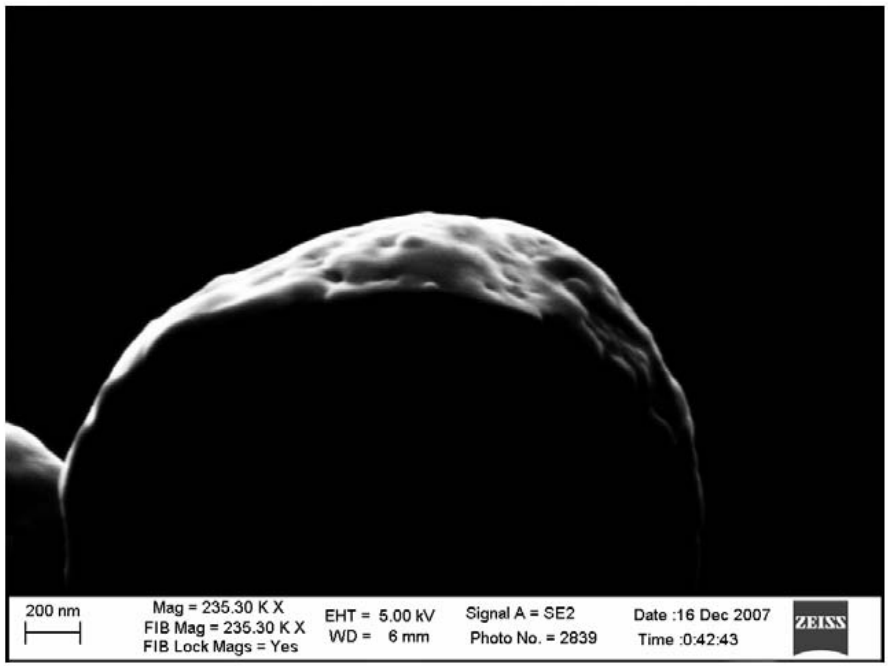

SEM image (SE2 detector) $MgAl_2O_4$ thickness variation on the Mo Surface

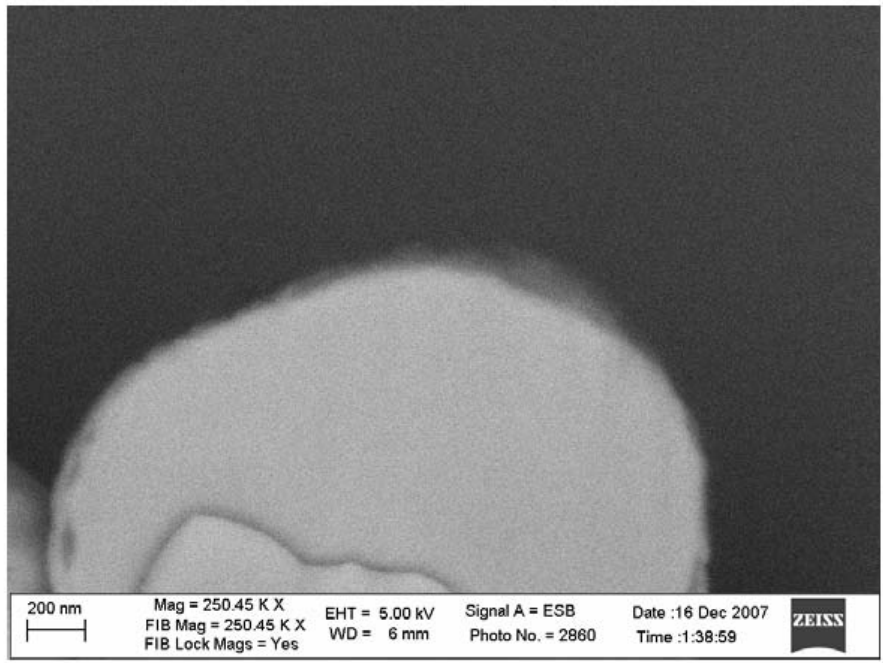

ESB image: bright areas are Mo and less bright cover is $MgAl_2O_4$

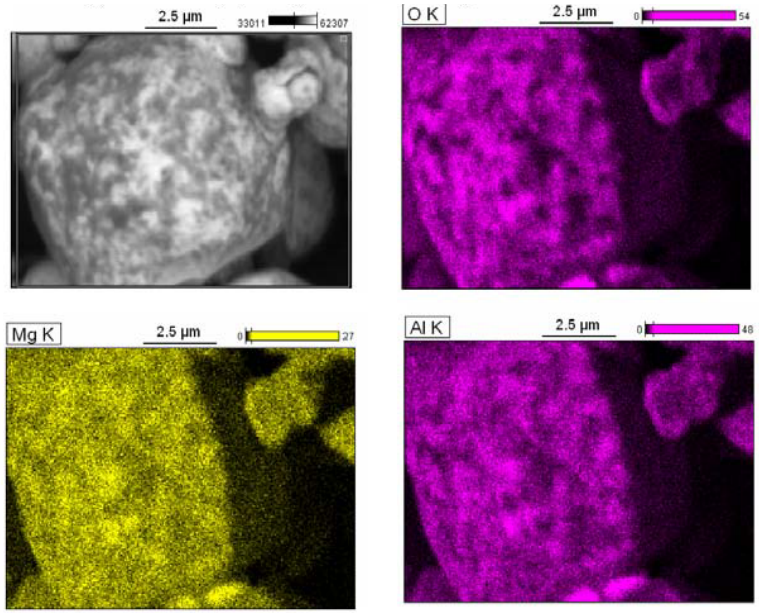

EDS maps (O, Mg, Al, Mo): confirm $MgAl_2O_4$ on Mo particle surface. Brighter areas (top left) have less $MgAl_2O_4$.

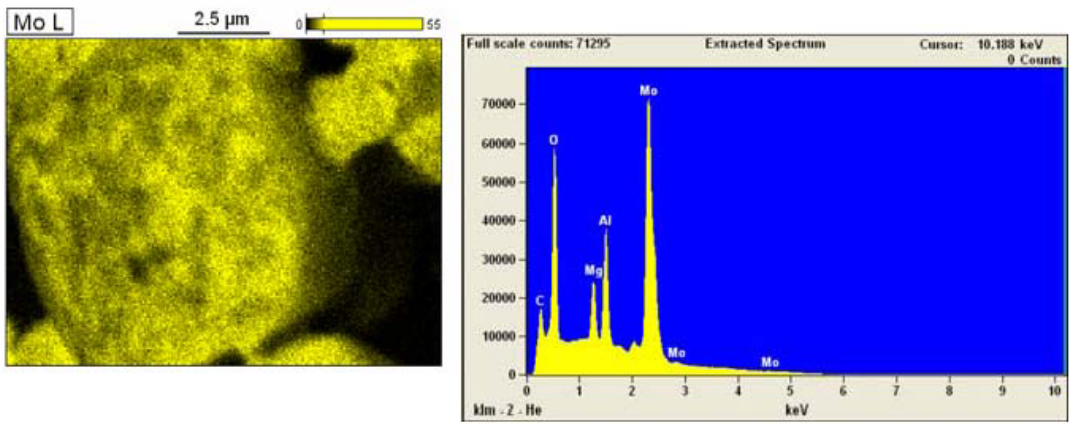

EDS spectrum from the whole area: Mo, Al, Mg, O

Bending Of Mo+$MgAl_2O_4$ (MCB processing)

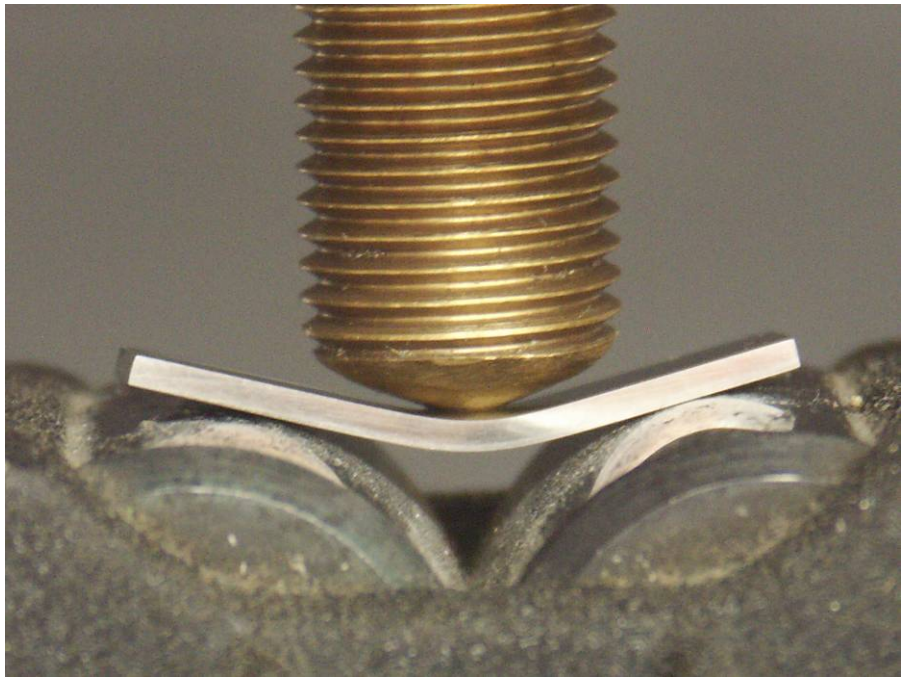

Specimen under loading

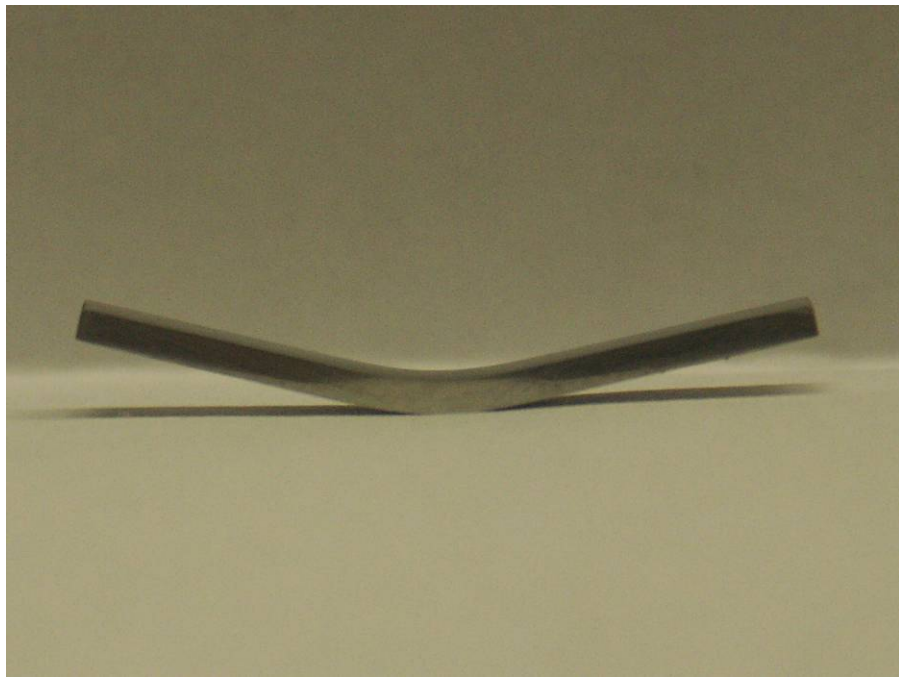

Specimen after unloading

- Vickers hardness
  (plastic flow observed)

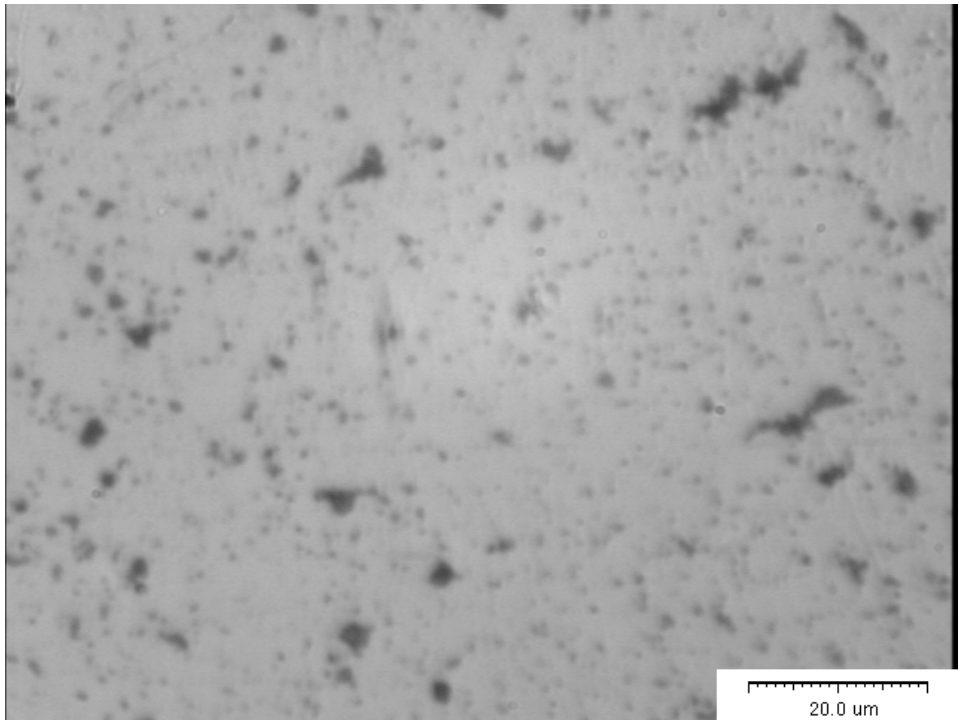

Microstructure

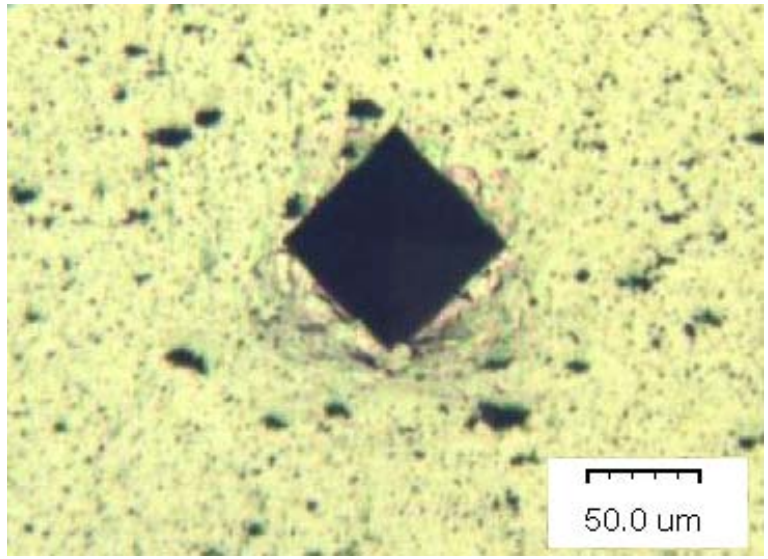

225HV, 1kg, 30s, 10x

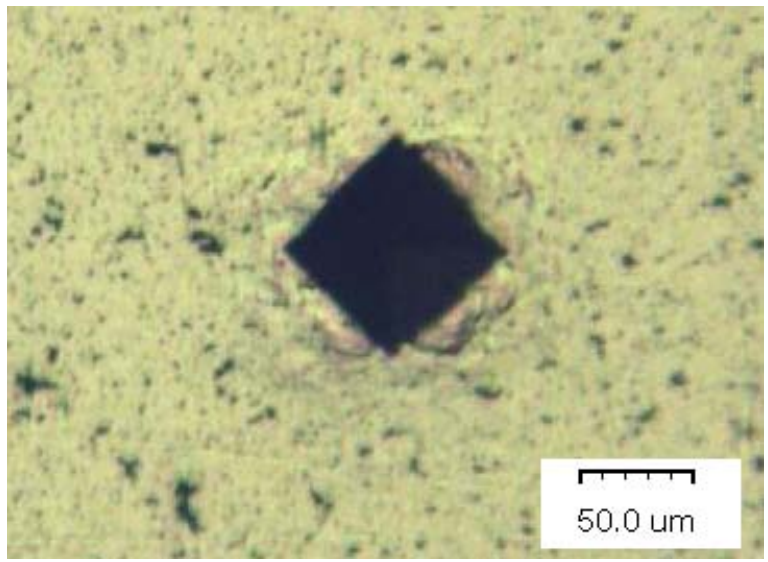

230HV, 1kg, 30s, 10x

Comparison of Ductility through Vickers Indentation

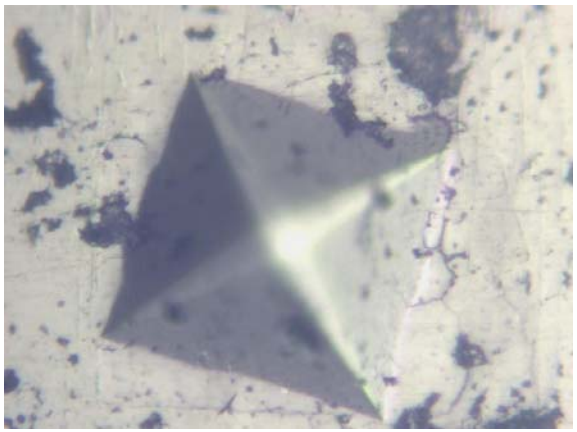

#697: Cracks observed

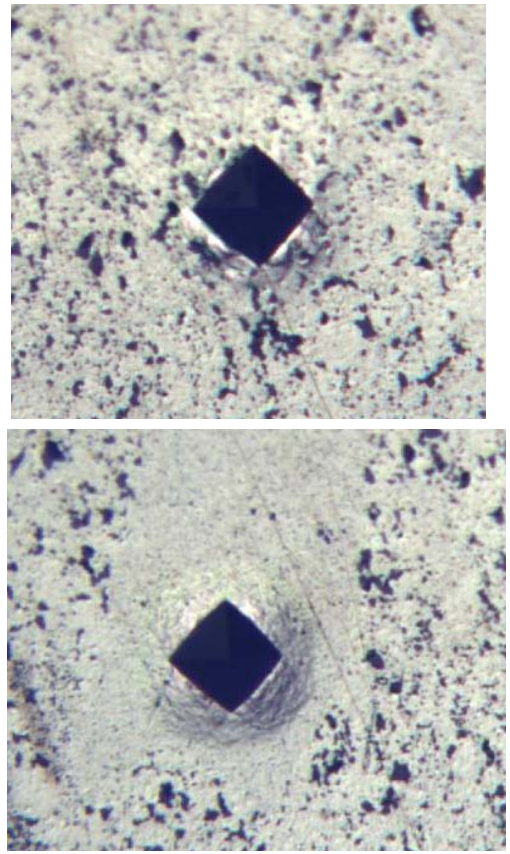

Mo-Nano $MgAl_2O_4$ with sonication process (WVU)

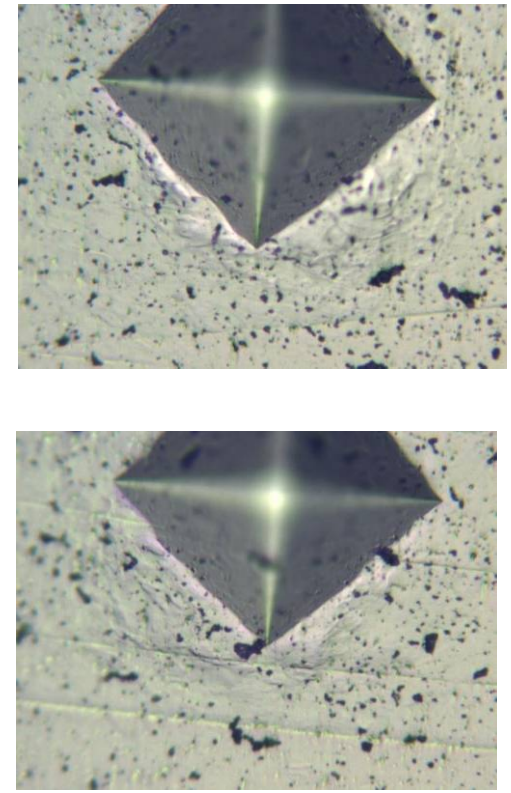

Mo-Nano $MgAl_2O_4$ with MCB process (WVU)

Conclusion:

Task 1: Molecular Dynamic Simulation

- Identified ***microscopic*** criteria to predict **brittle/ductile** properties. *These criteria can explain the **mechanisms** and be used in larger scale simulations to **optimize** performance*
- Observed possible tendency for **impurity gettering.** *This work demonstrates the capability of studying the **dynamic effects** and carrying out large scale simulations*

Task 2: In-situ Mechanical Property Measurement

- Developed a micro-indentation technique for **in-situ mechanical property** measurement.
- Mechano-Chemical Bonding (MCB) process can **bond nano-size particles** onto the surfaces of larger host particles to achieve desirable **uniform dispersing of the nano-sizes oxides in the alloy matrix**. Preliminary results show evidences of using the MCB processing technique to produce **cost-effective** Mo alloys with improved room-temperature ductility.

Thank You

Development of a Portable Transparent Indenter Micro-indentation Instrument with Integrated Spectroscopy and Surface Morphology Measurement

- To develop a portable Transparent Indenter Micro-indentation (TIM) Instrument which can evaluate not only mechanical properties but also the corresponding chemical composition, residual stress state and surface morphology of the tested material through integrated micro-indentation, laser fluorescence spectroscopy and imaging technologies.

- By embedding a CMOS sensor and employing innovative optical design, an optically transparent indenter assembly is integrated with (a) a PZT actuator and a miniature load cell for material micro-indentation tests, (b) an on-line fiber optic laser spectroscopy assembly for fluorescence spectroscopy measurement, and (c) a CMOS imaging module for high fidelity surface morphology mapping.

- The featured transparent indenter serves as a conduit for simultaneous in-situ surface morphology imaging, chemical composition identification and residual stress evaluation while under mechanical indentation testing.

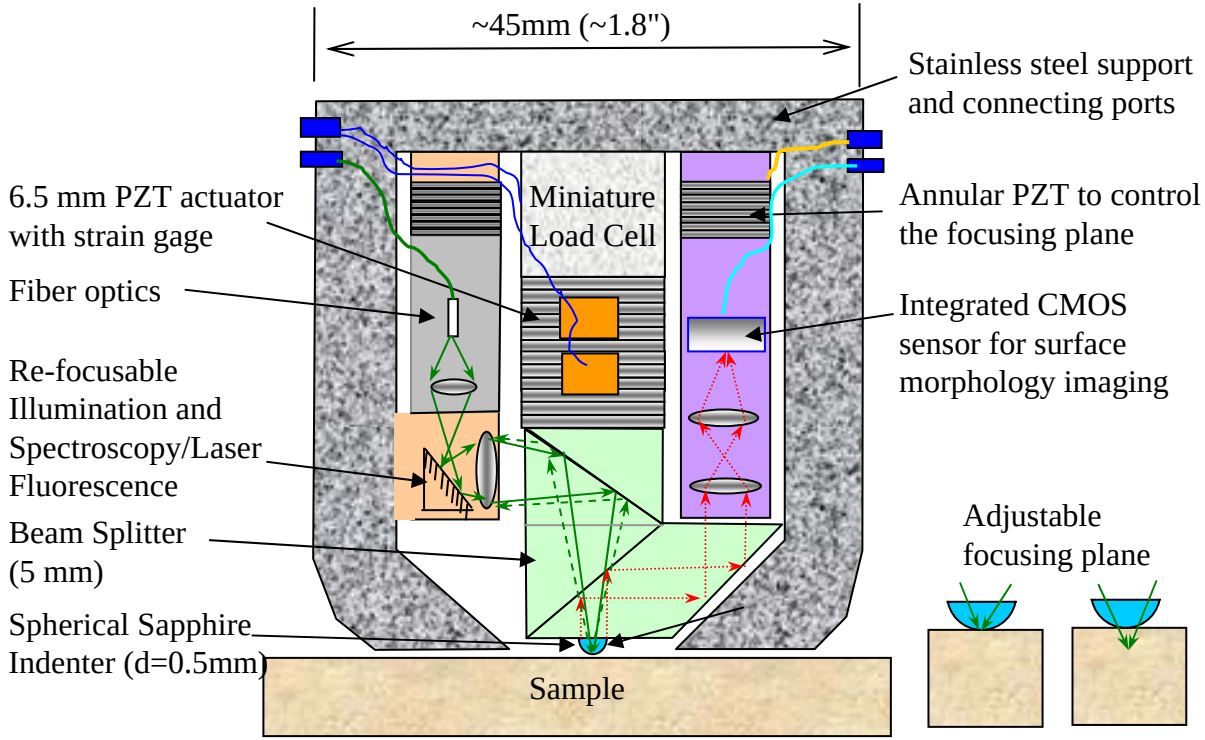
~45mm (~1.8")
Stainless steel support and connecting ports
6.5 mm PZT actuator with strain gage
Miniature Load Cell
Annular PZT to control the focusing plane
Fiber optics
Integrated CMOS sensor for surface morphology imaging
Re-focusable Illumination and Spectroscopy/Laser Fluorescence
Beam Splitter (5 mm)
Spherical Sapphire Indenter (d=0.5mm)
Sample
Adjustable focusing plane

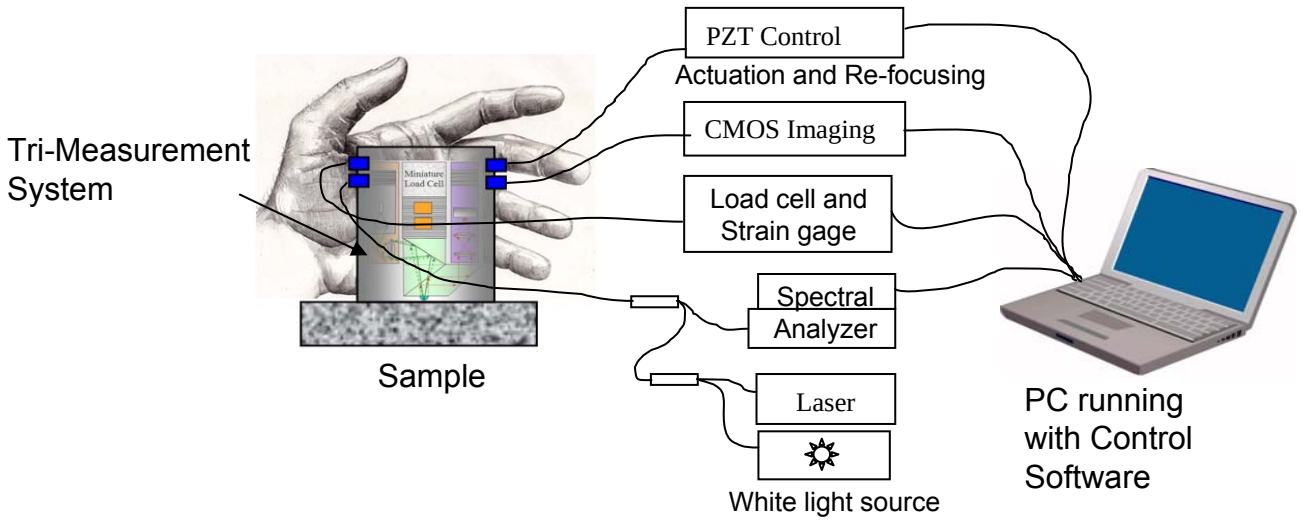
Tri-Measurement System
PZT Control
Actuation and Re-focusing
CMOS Imaging
Load cell and Strain gage
Spectral Analyzer
Laser
White light source
Sample
PC running with Control Software